RF/Microwave Absorbing Nanoparticles and Hyperthermia

by

Jason Ray Cook, B.S.

Thesis

Presented to the Faculty of the Graduate School

of the University of Texas at Austin

in Partial Fulfillment

of the Requirements

for the Degree of

Masters of Science in Engineering

The University of Texas at Austin

December 2009

The Thesis committee for Jason Ray Cook certifies that this is the approved version of the following thesis:

RF/Microwave Absorbing Nanoparticles and Hyperthermia

Approved by
Supervising Committee:

Supervisor: _____

Stanislav Y. Emelianov

_____

John A. Pearce

Dedication

This thesis is dedicated to my loving parents,

who battled all adversity,

so that I could have an education.

And my little brother,

who always challenged me,

to become the person I am today!

Acknowledgements

First and foremost I would like to thank Dr. Stanislav Emelianov for his advice, support, and patience during my graduate study. His magnanimous nature allowed me to select my area of research and pursue endeavors that were beneficial. Secondly, I would like to thank Dr. John Pearce for his patience and insight. He cordially passed some of his experience in electrical engineering and diathermy with great passion. Finally, for their tireless help and discussions I would like to thank my lab mates: Dr. Jignesh Shah, Seungsoo Kim, Mohammad Mehrmohammadi, Dr. Salavat Aglyamov, Jimmy Su, Dr. Andrei Karpiouk, Dr. Suhyun Park, Srivalleesha Mallidi, Bo Wang, Seung Yun Nam, Kimberly Homan, Pieter Kruizinga, Erika Cooley, Min Qu, Katherine Wilson, Soon Joon Yoon, Sangpil Yoon, Yun-Sheng Chen, Pratixa Joshi, and Tera Sherrard.

RF/Microwave Absorbing Nanoparticles and Hyperthermia

by

Jason Ray Cook, M.S.E.

The University of Texas at Austin, 2009

SUPERVISOR: Stanislav Y. Emelianov

The primary purpose of this work was to evaluate the capability of nanoparticles to transform electromagnetic energy at microwave frequencies into therapeutic heating. Targeted nanoparticles, in conjunction with microwave irradiation, can increase the temperatures of the targeted area over the peripheral region. Therefore, to become clinically viable, microwave absorbing nanoparticles must first be identified, and a system to monitor the treatment must be developed.

In this study, ultrasound temperature imaging was used to monitor the temperature of deep lying structures. First, a material-dependent quantity to correlate the temperature induced changes in ultrasound images (i.e. apparent time shifts) to differential temperatures was gathered for a tissue-mimicking phantom, porcine *longissimus dorsi* muscle, and porcine fat. Then microwave nanoabsorbers were identified using an infrared radiometer. The determined nanoabsorbers were then injected into *ex-vivo* porcine *longissimus dorsi* muscle tissue. Ultrasound imaging

frames were gathered during microwave treatment of the inoculated tissue. Finally, the ultrasound frames were analyzed using the correlation between temperature and apparent shifts in ultrasound for porcine muscle tissue. The outcome was depth-resolved temperature profiles of the *ex-vivo* porcine muscle during treatment.

The results of this study show that magnetite is a microwave nanoabsorber that increases the targeted temperature of microwave hyperthermia treatments. Overall, there is clinical potential to use microwave nanoabsorbers to increase the efficiency of microwave hyperthermia treatments.

Table of Contents

Chapter 1: Introduction

Despite tremendous monetary investment and research efforts, cancer remains the second leading cause of death in the United States with 1 in 2 men and 1 in 3 women at risk of contracting the disease during their lifetime [1]. Between 1996 and 2004 the 5-year relative survival rate for all diagnosed cancers is 66%, up from 50% in 1975-1977. This is primarily due to the advancements in early stage detection [1]. During the late 1970's through the early 1980's a cancer ablation technique that involves elevating tissue temperatures above 42˚C was widely explored. The research of this form of therapy, known as hyperthermia, peaked due to an inability to noninvasively focus heat exclusively to the tumor. Focusing heat is important because of the how hyperthermia effects cells. In the temperature range of hyperthermia, all cells are not instantly destroyed; rather, the proportion of cells destroyed depends on treatment duration, treatment temperature, cancer cell line, and micro-environmental factors [2].

Several treatment modalities exist in cancer hyperthermia therapy, such as: high intensity focused ultrasound (HIFU), photothermal, whole body, radiofrequency (RF) therapy, and microwave therapy. HIFU utilizes high intensity ultrasound transducer to thermally induce cell death by mechanical movement of the focal zone [3]. Due to the conical nature of acoustic focus, there are spatially large temperature gradients when treating deep structures. Another problem with HIFU is that it must utilize imaging to guide therapy. Photothermal therapy utilizes lasers to achieve hyperthermia conditions.

With the recent addition of targeted nanoparticles, the laser energy can primarily be focused at the cancer without the need of imaging [4-7]. However, maximal treatment depths are limited to around 1 cm [4,8]. Whole body hyperthermia is the elevation of the entire body temperature to treat cancer. This technique and can treat deep seated cancers. On the other hand, neuronal tissue damage, splanchnic dilation, hypotension, circulatory shock, and dehydration can occur with this technique [9,10]. RF and microwave therapy utilize non-ionizing electromagnetic radiation, usually above audible frequencies (>20 kHz) to 100 GHz. RF and microwave therapy have proven effective with minimal complications for several types of cancers [11-15]. In addition, RF therapy can treat deep seated cancers due to minimal attenuation in the body. Microwave catheters allow for treatment of deep seated cancers with minimal invasion. However, RF and microwave therapy both utilize either proximal placement of applicators or electromagnetic property differences between cancerous and normal tissues to induce targeted ablation.

Ideally, hyperthermia therapy will involve non-invasive, non-ionizing application of heat at any depth of the body with minimal normal tissue heating. Therefore, coupling targeted RF or microwave absorbing nanoparticles with an applied RF or microwave field will allow for focused energy deposition. RF and microwave energy can be focused or redirected by using materials that absorb the electromagnetic energy [16-18]. This phenomenon could not be exploited in RF and microwave hyperthermia until the recent fabrication of nanoparticless. Nanoparticles are widely used in medicine today, primarily in the field of medical imaging. MRI utilizes targeted

iron-oxide nanoparticles to provide contrast in tissue structures. Nanoparticles are also currently used in drug delivery, tissue engineering, and cell separation. In addition, medical research involving nanoparticles has extended to ultrasound imaging, radiographic imaging, optical imaging, bio-detection, and hyperthermia, just to name a few [19].

1.1 Cancer

Cancer is a general term referring to the abnormal growth of cells. Cancer often arises due to genetic changes or damage to a chromosome within a cell. These mutations can be caused by improper cell division, bacteria, radiation, certain hormones and drugs, viruses, etc [20]. The mutated gene sends an incorrect message that causes the cell to grow rapidly until a lump forms. Uncontrolled rapid cell growth is unlike normal rapid cell growth because genes do not exist to tell the mass to stop growing. Cancerous masses inhibit normal physiological function through direct or indirect strain on a process.

Cancers usually grow from a single site, known as a primary site. Therefore, cancer usually spreads because small fragments of cancerous cells are cast from the primary site and travel to other parts of the body (metastasis). One process of cancer spread is known as direct extension. As tumor masses grow, it invades the organs and adjacent tissues. Another process of cancer spread is through the blood. The circulatory system extends throughout the body and is a prime transportation system to allow metastasis. The final means for cancer metastasis is through the lymphatic

system. Like the circulatory system, the lymphatic system extends throughout the body and can easily distribute cancer cells.

There are four different types of tumors: carcinomas, sarcomas, lymphomas, and leukemias. Carcinomas develop in tissues that cover the surface or line internal organs and passageways [20]. Most carcinomas develop in organs that are involved in secretion (lungs, breasts, pancreas, etc.). Sarcomas develop in any supporting or connective tissues (muscles, bones, nerves, tendons, or blood vessels) [20]. Lymphomas develop in lymph glands and are usually always malignant [20]. Leukemias are cancers of the white blood cells and plasma cells [20].

1.2 RF/Microwave Heating in Living Systems

Electromagnetic (EM) waves within the 1 MHz to 100 GHz spectrum have special biological significance since they can readily be transmitted through, absorbed by, and reflected at biological tissue boundaries [21]. The primary mechanism of RF and microwave power on biological tissues is the transformation of the introduced electromagnetic energy into increased kinetic energy within the absorbing molecules, thereby heating the tissues [21]. The heating results from ionic conduction and movement of the dipole molecules, such as water. The amount of heating depends on many factors, such as: tissue perfusion, tissue geometry, tissue dielectric properties, tissue heat transfer properties, source frequency, source power, applicator configuration, and applicator geometry.

1.2.1 Attenuation of Electromagnetic Waves in Tissue

One aspect of EM wave propagation in tissue is the attenuation of energy with depth. For propagation in a homogeneous complex lossy media (energy absorbing dielectric), Maxwell's equations reduce to the vector Helmholtz equations:

$$\nabla^2\vec{E} - \gamma^2\vec{E} = 0, \tag{1.1}$$

$$\nabla^2\vec{H} - \gamma^2\vec{H} = 0, \tag{1.2}$$

where $\vec{E}$ is the electric field, ∇^2 is the Laplacian operator, and γ is the complex propagation constant $\gamma = \alpha + j\beta$, where α is the attenuation coefficient and β is the phase coefficient. The attenuation and phase coefficients are defined as:

$$\alpha = \omega\sqrt{\mu^*\varepsilon^*}\left\{\frac{1}{2}\left[\sqrt{1+\left(\frac{\sigma_{eff}}{\omega\varepsilon^*}\right)^2} - 1\right]\right\}^{\frac{1}{2}}, \tag{1.3}$$

$$\beta = \omega\sqrt{\mu^*\varepsilon^*}\left\{\frac{1}{2}\left[\sqrt{1+\left(\frac{\sigma_{eff}}{\omega\varepsilon^*}\right)^2} + 1\right]\right\}^{\frac{1}{2}}, \tag{1.4}$$

where ω is the angular frequency $2\pi f$, μ^* is the complex magnetic permeability $\mu^* = \mu_0\mu_r^{'} - j\mu_0\mu_r^{''}$, μ_0 is the magnetic permeability in free space $4\pi\ x\ 10^{-7}\ \frac{H}{m}$, ε^* is the complex electrical permittivity $\varepsilon^* = \varepsilon_0\varepsilon_r^{'} - j\varepsilon_0\varepsilon_r^{''}$, ε_0 is the electrical permittivity in free space $\sim 8.854\ x\ 10^{-12}\ \frac{F}{m}$, and σ_{eff} is the effective conductivity $\sigma + \omega\varepsilon^{''}$. For biological tissues the imaginary portion of the magnetic permeability is negligible. However, due to polar protein molecules and the polar nature of water, the imaginary portion of the electrical permittivity, also known as known as the dielectric losses, is a major source of heating at RF and microwave frequencies.

Revisiting the Helmholtz equations (1.1) and (1.2) for a uniform plane wave with the electric field is polarized in the x-direction, the magnetic field is in the y-direction, and the propagation is in the z-direction, solutions are the following:

$$E_x(z,t) = E_{x\,0}^{+} e^{-\alpha z}\cos(\omega t - \beta z) + E_{x\,0}^{-} e^{+\alpha z}\cos(\omega t + \beta z), \qquad (1.5)$$

$$H_y(z,t) = H_{y\,0}^{+} e^{-\alpha z}\cos(\omega t - \beta z) - H_{y\,0}^{-} e^{+\alpha z}\cos(\omega t + \beta z), \qquad (1.6)$$

where the + superscript denotes forward propagating fields and the – superscript denotes backward propagating fields. The electrical permittivity ε^* and the magnetic permeability μ^* are frequency-dependent, as shown by Debye in 1923 [22]. Therefore, the attenuation is frequency dependent. For forward propagating fields, the most common case, the attenuation of energy follows an $e^{-\alpha z}$ relationship. The nature for this pattern of energy loss in tissue is shown in Figure 1.1.

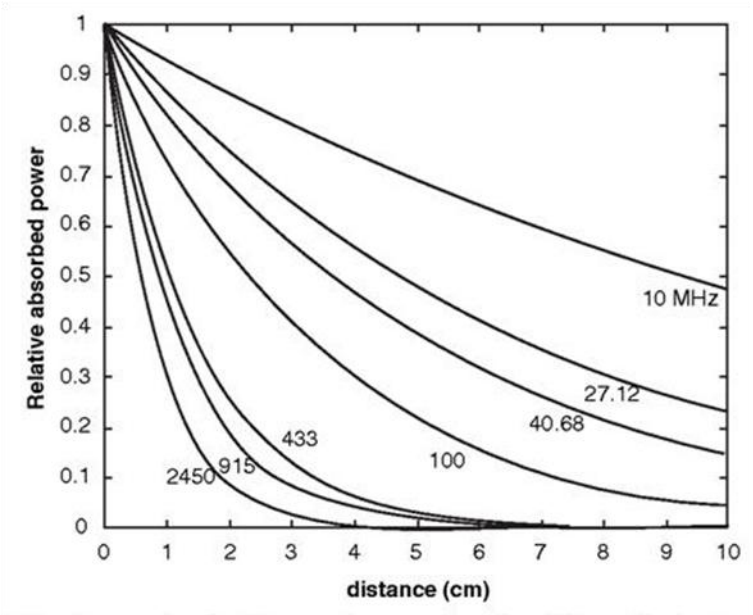

Figure 1.1: Relative absorbed power versus penetration depth of muscle tissue from 10 to 2.45 GHz [23].

1.2.2 Reflection of Electromagnetic Waves in Tissue

Since fat, muscle, bone, brain, skin, etc. have different electrical and magnetic properties, general reflections between various tissue interfaces will occur when exposed to RF/microwave waves. The characteristic impedance of a medium is:

$$\eta = \sqrt{\frac{j\omega\,\mu^*}{\sigma + j\omega\,\varepsilon^*}}. \tag{1.7}$$

The characteristic impedance relates the electric field to the magnetic field:

$$H_{y\,0}^{+} = \frac{E_{x\,0}^{+}}{\eta}\ , H_{y\,0}^{-} = \frac{E_{x\,0}^{-}}{\eta}. \tag{1.8}$$

If a uniform plane wave is propagating in one medium (1) and encounters a second medium (2), then the total field in medium 1 is the sum of the incident and reflected waves:

$$\vec{E}_1(z,\omega) = E_i\left(e^{-j\beta_1 z} + \Gamma e^{+j\beta_1 z}\right)\vec{a}_x, \tag{1.9}$$

$$\vec{H}_1(z,\omega) = \frac{E_i}{\eta_1}\left(e^{-j\beta_1 z} + \Gamma e^{+j\beta_1 z}\right)\vec{a}_y, \tag{1.10}$$

where E_i denotes the electric field strength of the incident wave and the electric field reflection coefficient Γ is:

$$\Gamma = \frac{\mathrm{E_r}}{\mathrm{E_i}} = \frac{\eta_2 - \eta_1}{\eta_2 + \eta_1}, \tag{1.11}$$

where $\mathrm{E_r}$ is the electric field strength of the reflected wave. The transmitted wave in medium 2 is:

$$\vec{E}_2(z,\omega) = E_i T e^{-j\beta_2 z}\vec{a}_x, \tag{1.12}$$

$$\vec{H}_2(z,\omega) = \frac{E_i}{\eta_2} T e^{-j\beta_2 z}\vec{a}_y, \tag{1.13}$$

where the electric field transmission coefficient T is:

$$\Gamma = \frac{E_t}{E_i} = \frac{2\eta_2}{\eta_2+\eta_1}, \quad (1.14)$$

where E_t is the electric field strength of the transmitted wave. When a large reflection coefficient exists, such as between low water content tissue and high water content tissue (fat to water interface), the wave is reflected nearly 180˚ out of phase with the incident wave [21]. This can produce a standing wave, as shown in Figure 1.2, where the relative absorbed power follows a non-predictive pattern in the fat layer.

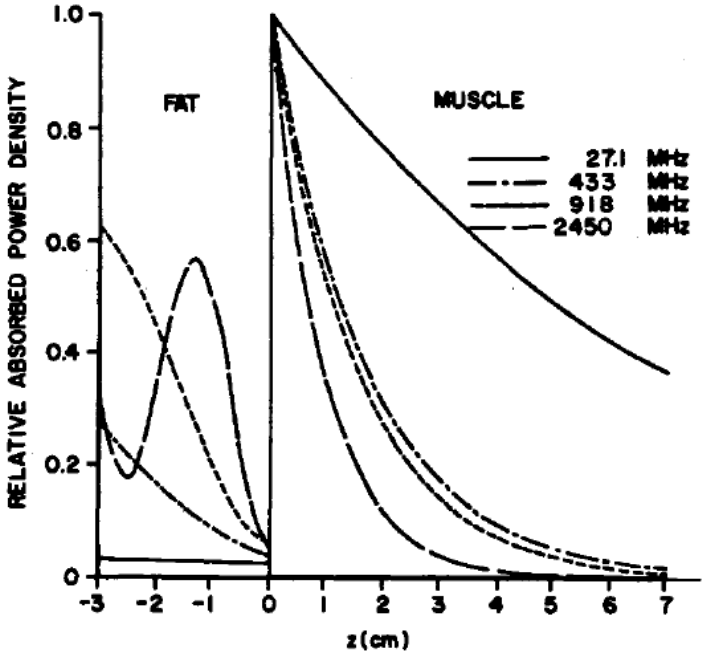

Figure 1.2: Relative absorbed power density patterns in plane fat and muscle layers exposed to plane waves [21].

Therefore, the tissue layer thickness plays an important role in the absorption pattern of the electromagnetic energy.

1.2.3 The Poynting Power Theorem

Heat generation in tissues due to electromagnetic irradiation is characterized by the Poynting Power Theorem. This theorem includes the effects of both displacement current and magnetic induction. In the frequency domain, the local power density in a propagating wave is represented in the Poynting vector:

$$\vec{S}(\omega) = \frac{1}{2}\left(\vec{E}(\omega) \times \vec{H}^{*}(\omega)\right), \tag{1.15}$$

where the * indicates the complex conjugate of $\vec{H}$. Therefore, the magnitude of absorption is:

$$-\vec{\nabla} \cdot \vec{S}(\omega) \approx (\sigma + \omega\varepsilon^{*})\left|\vec{E}\right|^{2} + j\omega\mu^{*}\left|\vec{H}\right|^{2}. \tag{1.16}$$

where the negative sign indicates that power is absorbed from the electromagnetic field. Heating from electromagnetic irradiation of tissue is given by the real part of equation (1.16):

$$Q_{gen} = Re\left\{-\vec{\nabla} \cdot \vec{S}(\omega)\right\} \approx (\sigma + \omega\varepsilon^{''})\left|\vec{E}\right|^{2} + \omega\mu^{''}\left|\vec{H}\right|^{2}. \tag{1.17}$$

Q_{gen} is the source term in the bioheat energy balance, as shown in the following section.

1.3 Damage Assessment

The ability to correlate treatment temperature and treatment duration to cell death is important in any form of hyperthermia therapy. A quick treatment at high temperatures will yield the same number of dead cells as a long treatment at low temperatures. This concept is shown in two damage assessments: the Arrhenius reaction kinetics model and the cumulative equivalent minutes at 43˚C model. Before achieving a quantitative measurement of cell death, knowledge of heat transfer in tissues must be known.

1.3.1 Heat Transfer in Tissues

One of the most fundamental laws of nature is the First Law of Thermodynamics, also known as the conservation of energy. This law states that during an interaction, energy can change from one form to another but the total energy remains constant ($E_{in} - E_{out} + E_{initial} = 0$) [24]. This law is very important in hyperthermia because the conservation of energy allows for a quantitative measure of heat in tissues. Harry H. Pennes' paper titled "Analysis of tissue and arterial blood temperatures in the resting human forearm" detailed an early attempt to adapt the First Law of Thermodynamics [25]. Pennes' principal theoretical contribution was his method to simplify the mass heat transport performed by blood [26]. This relationship is as follows:

$$h_b = w\rho_b C_b(1-\kappa)(T_a - T), \tag{1.18}$$

where h_b is the rate of heat transfer per unit volume of tissue, w is the perfusion rate per unit volume of tissue, ρ_b is the density of blood, C_b is the specific heat of blood at constant volume, κ is a factor that accounts for incomplete thermal equilibrium between blood and tissue, T_a is the arterial blood temperature, and T is the local tissue temperature [26]. Pennes assumed that $0 \leq \kappa \leq 1$; however, he set $\kappa = 0$ when he computed his theoretical curves, as have most subsequent investigators [26]. Using Penne's contribution, the heat energy balance becomes:

$$\rho_t C_t \frac{\partial T}{\partial t} = \nabla \cdot (k_t \nabla T) + Q_{gen} + Q_{met} + w\rho_b C_b(T_a - T), \tag{1.19}$$

where the subscript t represents tissue, k_t is the thermal conductivity of the tissue, and m is the mass of the control volume.

1.3.2 Arrhenius Reaction Kinetics

Moritz and Henriques produced a series of papers in the *American Journal of Pathology* in 1947 titled "Studies of Thermal Injury" which characterized kinetic models for irreversible thermal alterations in human and porcine skin [27-29]. Their seminal work is often used as the basis for numerical studies of tissue damage [30]. This model calculates a non-dimensional parameter, Ω, which is a logarithmic proportion of damaged cells:

$$\Omega(\tau) = \int_0^{\tau} \mathrm{Ae}^{\left[-\frac{\mathrm{E_a}}{\mathrm{RT\,(t)}}\right]} dt = \ln\left\{\frac{C(0)}{C(\tau)}\right\}, \tag{1.20}$$

where A is a measure of the effective collision frequency between reacting molecules in bimolecular reactions in s^{-1}, E_a is the activation energy barrier that molecules must surmount to transform from the native to damaged state in $\frac{J}{mole}$, R is the universal gas constant $8.314\frac{J}{mole\ K}$, T is the temperature in K, $C(0)$ is the initial concentration of undamaged molecules, and $C(\tau)$ is the concentration of damaged molecules [30]. Values for A and E_a for various tissues have been proposed by several investigators [30-59]. At any time during the heat exposure, the probability of damaged proteins can be predicted from:

$$P(\%) = 1 - C(\tau) = 100[1 - e^{-\Omega}]. \tag{1.21}$$

Since denatured protein molecules can equate to dead cells, the equations (1.20) and (1.21) can provide a basis to predict cell death.

1.3.3 Cumulative Equivalent Minutes at 43˚C (CEM 43)

CEM 43 is a thermal dose measure to correlate the synergism between treatment temperature and treatment duration. The significance of 43˚C is that this is an experimental break point temperature in cell survival studies, above which the surviving fraction of cells decrease significantly [31]. This break point is illustrated in Figure 1.3.

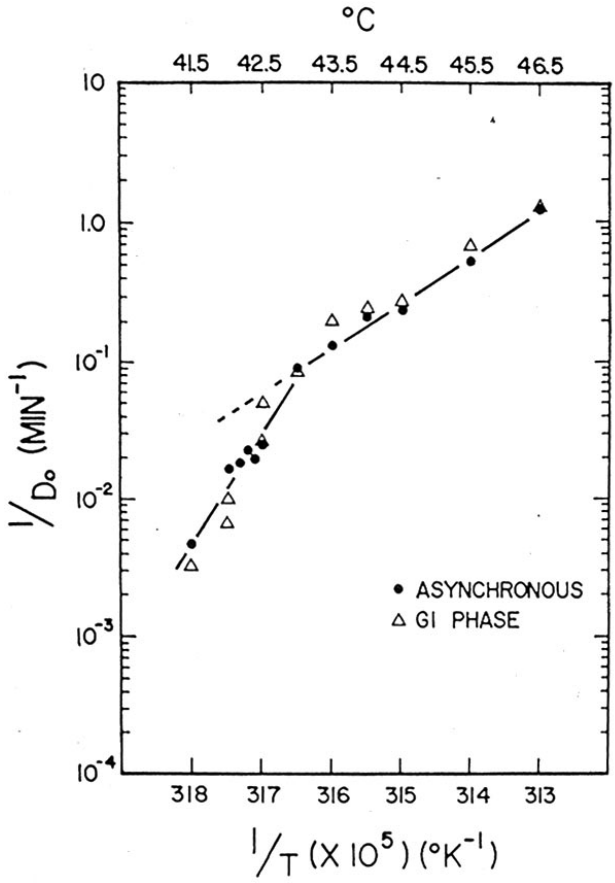

Figure 1.3: Survival curves for Chineses hamster ovarie cells (CHO) [31].

The physical significance of D_0 is that it is the time at which $\Omega = 1$, or the surviving fraction of cells is e^{-1} times as small from the original number.

Utilizing curves like that shown in Figure 1.3, CEM 43 can be calculated from the following relationship:

$$CEM\ 43 = \int_0^{\tau} R^{(T_{break}\ -T(t))} dt, \tag{1.22}$$

where R is a parameter characterizing the damage accumulation, T_{break} is the break point (most commonly 43˚C), $T(t)$ is the tissue temperature at time t, and τ is the total treatment time [30]. R can be determined from the following relationship [30]:

$$\ln\{\mathrm{R}\} = \frac{\ln\left\{\frac{D_0(T_{break})}{D_0(T)}\right\}}{T_{break}\ -T}. \tag{1.23}$$

From Figure 1.3, it is obvious that R will have two different values, one value for temperatures above the break point and another for values below the break point. Typical values for R are around 0.25 for temperatures less than 43˚C and 0.5 for temperatures greater than 43˚C [31].

1.4 Treatment Monitoring

Much like radiotherapy, a successful hyperthermia treatment must rely on the ability to monitor dosimetry. Instead of controlling dosimetry with total exposure time, RF/microwave therapy relies on the ability to monitor tissue temperatures. One approach is to invasively implant a temperature sensor such as an optical probe thermometer. Thermocouples and thermisitors cannot be used with RF/microwave field exposures because their metallic construction absorbs the EM energy and changes the

temperature distribution within the tissue. Several noninvasive temperature monitoring modalities exist, such as infrared cameras, magnetic resonance imagers (MRI's), and ultrasound imagers. Infrared cameras are often used for surface imaging because of the depth-limited (~25 μm) emission of infrared energy in biological tissues [60]. MRI tomography temperature monitoring (MRT) provides excellent resolution and can image deep-seated structures; however, the high cost associated with MRI and the bulky equipment hinders patent accessibility [2]. On the other hand, ultrasound temperature monitoring has less associated cost and can image deep-seated structures. In addition, thermal ultrasound imaging has been shown to measure temperature changes of less than 1˚C with a spatial resolution similar to diagnostic ultrasound imaging [61,62].

1.4.1 Ultrasound Imaging

Ultrasound imaging utilizes pressure waves to characterize spatial locations, mechanical properties, and physiological function of subcutaneous anatomy. Most modern ultrasound imaging scanners transmit an ultrasound pulse, usually at 3-15 MHz, into the body using a piezoelectric transducer array. The pressure wave then interacts with the tissues and some of the acoustical energy is reflected back to the transducer. This backscattered energy is converted to an electrical signal. Using the time delays in the backscattered pulses, the position of the subcutaneous structures can be determined.

Deep tissue temperatures can be monitored using ultrasound imaging by tracking the thermal-motion of speckle [62-67]. This thermal-motion, or apparent time shift, is primarily caused by the temperature dependency of the speed of sound of tissue,

while the thermal expansion is negligible for temperatures below 60˚C [68]. The spatial location in ultrasound images is dependent on the speed of sound, and for a homogeneous medium, the time of echo is given by:

$$t(T) = \frac{2z}{c(T)}, \tag{1.24}$$

where t is the time delay of echo from the scatterer at position z with a temperature of T and $c(T)$ is the temperature dependent speed of sound of the medium.

If the temperature of the medium is increased by ΔT, then there is an apparent time shift in the ultrasound signal due to the combined effects of the temperature dependent speed of sound and the thermal expansion of the tissue. For a homogeneous medium, new time of echo is expressed as:

$$t(T_0 + \Delta T) = \frac{2z(1+\alpha\Delta T)}{c(T_0+\Delta T)}. \tag{1.25}$$

where α is the linear coefficient of thermal expansion. Apparent time shifts, Δt, are primarily dependent on the speed of sound and thermal expansion is negligible below 60˚C [68]. Therefore, the apparent time shift becomes:

$$\Delta t = t(T_0 + \Delta T) - t(T_0) = 2z\left[\frac{1}{c(T_0+\Delta T)} - \frac{1}{c(T_0)}\right]. \tag{1.26}$$

Due to the Δt dependency on depth, a deep lying structure will experience a larger Δt than shallower structures. This effect is shown in Figure 1.4.

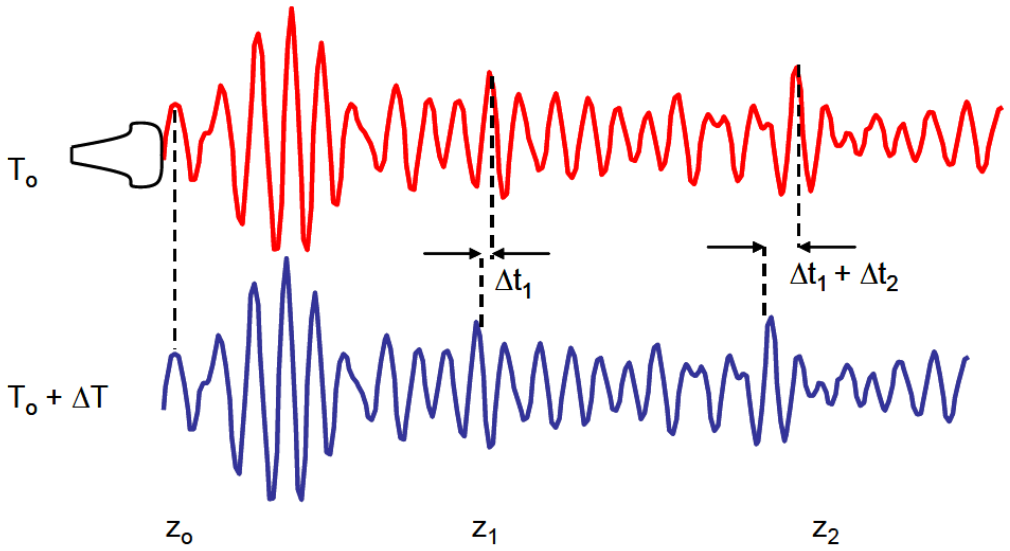

Figure 1.4: Temperature increase ($\Delta \boldsymbol{T}$) causes apparent time shifts ($\Delta \boldsymbol{t_1}$ and $\Delta \boldsymbol{t_1} + \Delta \boldsymbol{t_2}$) in the ultrasound echo captured at elevated temperature ($\boldsymbol{T_0} + \Delta \boldsymbol{T}$) [69].

The spatial dependence of Δt can be removed by differentiating along the axial direction. Thus, the differential temperature can be characterized with the following relationship:

$$\Delta T = k \frac{d(\Delta t)}{dt}, \tag{1.27}$$

where k is a material dependent property that is found experimentally and $\frac{d(\Delta t)}{dt}$ is the spatial gradient of Δt and is known as the normalized time shift [69].

1.5 Nanoparticles

Typically, nanoparticles (NPs) are defined as microscopic particles between 1 and 100 nm, or up to 1 μm as some investigators suggest. Nanoparticulate delivery systems in RF/microwave therapy can provide increased thermal absorption in cancers with reduced risk. For example, NPs less than 20 nm in size are able to pass through

blood vessel walls; thus, allowing for intravenous injections as well as intramuscular and subcutaneous applications [70]. In addition, the scale of NPs allows for interactions with biomolecules on the cell surfaces and within the cells, which do not necessarily alter the behavior and biochemical properties [70]. NPs can be targeted to seek cancer, thus aiding in the delivery of RF/microwave energy [70].

1.5.1 Electric Losses

One mode of RF/microwave energy conversion by NPs is Joule heating. Joule heating, also known as Ohmic heating or resistive heating, is caused by electron interactions with atomic ions that form the body of a conductor. Each electron/ion interaction causes electron kinetic energy loss in the form of heat dissipation. Joule heating is proportional to the power across a conductor:

$$Q_{gen} = \sigma_{eff} \left|\vec{E}\right|^2. \tag{1.28}$$

When nanoparticles with high electrical conductivities are placed in tissues, they direct the electromagnetic field, as shown in the Figure 1.5.

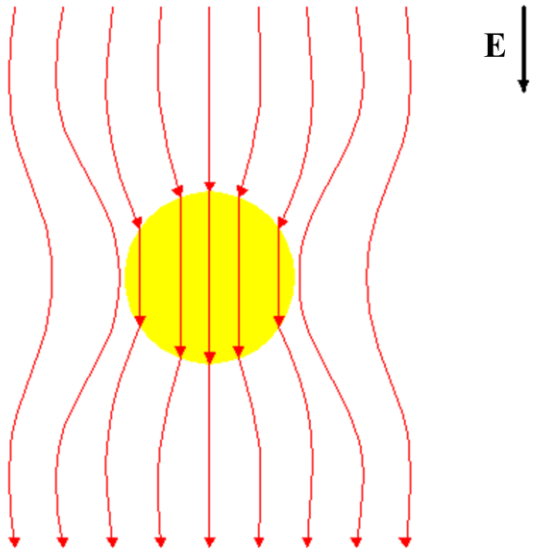

Figure 1.5: Electric field lines for a particle embedded within a uniform medium with $\sigma_{particle} >> \sigma_{medium}$.

Several investigators suggest that capacitively coupled nanoparticles induce heating of the surrounding tissue through thermal diffusion [71-73]. Although some Joule heating does occur within the particle, the primary source of tissue heating is from the Joule heating of the tissue itself. This is due to both the concentration of field around the particle and the substantially smaller electrical conductivity of the tissue.

1.5.2 Magnetic Losses

Magnetic heating usually utilizes magnetic oxides, such as iron oxides, because of their proven biocompatibility and significant energy dissipation when exposed to an alternating magnetic field [74]. The energy dissipation is either due to the loss processes during the reorientation of the magnetization or frictional losses if the particle can rotate in an environment of sufficiently low viscosity [74]. Losses due to

magnetization reorientation in ferro- and ferrimagnetic particles depend on the type of remagnetization process (wall displacements or several types of rotational processes) [73]. These are due to the intrinsic magnetic properties like magnetocrystalline anisotropy and exchange coupling constant (size, shape, microstructure, and grain size).

A. Néel Relaxation

Single domain (one grain structure) ferrous particles are superparamagnetic because by definition, each particle is a single magnetic domain. When single domain particles are exposed to alternating magnetic fields, one form of energy loss is due to the collective rotation of atomic magnetic moments within each particle. This phenomenon is known as Néel relaxation and is due to the energy barrier for magnetization reorientation, which is determined by the magnetocrystalline anisotropy [75]. Losses arising in superparamagnetic particles originate because there are only two metastable antiparallel orientations of the particle's magnetic moment m. The two corresponding energy levels are separated by an energy barrier due to the anisotropy energy KV (K is the anisotropic energy density, V is the particle volume). Assuming a high energy barrier compared to the observed macroscopic energy, $KV \gg k_b T$ (k_b is the Boltzmann constant, T is temperature), the relaxation time, τ, of the entire particle system is determined by the ratio of anisotropy energy KV to thermal energy $k_b T$:

$$\tau = \frac{\sqrt{\pi}}{2}\tau_0 \frac{e^{\left[\frac{KV}{k_b T}\right]}}{\sqrt{\frac{KV}{k_b T}}}, \tag{1.29}$$

where $\tau_0 \sim 10^{-9} s$ [75].

The volumetric power dissipation in an alternating magnetic field of amplitude H and frequency f is:

$$Q_{Neél} = \pi f \mu_0 H^2 \chi'', \tag{1.30}$$

where μ_0 is the magnetic permeability of free space and χ'' is the imaginary part of the magnetic susceptibility χ [76]. In the Debye model, the magnetic susceptibility for relaxation of magnetization with a characteristic time τ and angular frequency $\omega = 2\pi f$ is:

$$\chi'' = \frac{\omega\tau}{(1+(i\omega\tau)^2)}\chi_0, \tag{1.31}$$

where χ_0 is the static susceptibility and can be approximated by a Langevin relationship for small field amplitudes [75]:

$$\chi_0 = \chi_i \frac{3}{\xi}\left(\coth(\xi) - \frac{1}{\xi}\right), \qquad \xi = \frac{\mu_0 M_d H V}{k_b T}, \tag{1.32}$$

where ξ is the Langevin parameter, χ_i is the initial susceptibility, and M_d is the domain magnetization. For an adiabatic system the power loss relationship to temperature is defined by:

$$\Delta T = \frac{P\Delta t}{\rho c_p}, \tag{1.33}$$

where ρ is the weighted density of the particle material and c_p is the weighted specific heat capacity.

B. Brownian Relaxation

Brownian relaxation in can occur in single domain particles in an alternating magnetic field when the magnetic moment direction is strongly coupled to the particle's

geometry. That is, a large value of the intrinsic magnetic anisotropy combined with easy particle reorientation due to a low viscosity η of the medium surrounding the particle [78]. For particles with a hydrodynamic radius of r_h, the Brownian relaxation time is given by:

$$\tau_B = \frac{8\pi\eta r_h^3}{k_b T}. \quad (1.34)$$

Since Néel and Brownian relaxations occur in parallel (Figure 1.6), the effective relaxation time is given by:

$$\tau_{eff} = \left[\frac{1}{\tau_N} + \frac{1}{\tau_B}\right]^{-1}. \quad (1.35)$$

The effective relaxation time can be used in equation (1.31) for the calculation of the power dissipative losses.

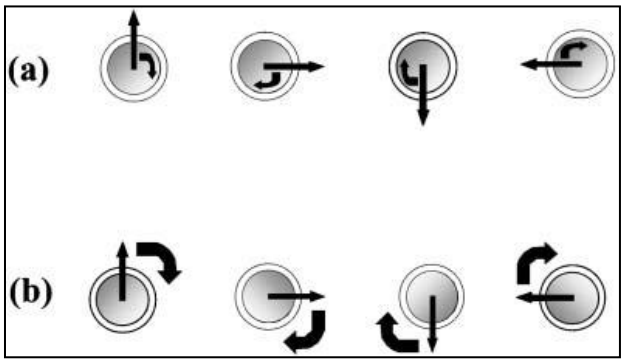

Figure 1.6: (a) Neél rotation of magnetization in a magnetic particle (the particle does not rotate); (b) Brownian rotation of the particle (the particle physically rotates) [75].

C. Magnetic Hysteresis

In multidomain (multiple grain structures per particle) ferro- and ferrimagnetic nanoparticles exposed to alternating magnetic fields, heating is dominated by hysteresis

losses. Each particle contains several subdomains (grain structures), each of which have their own definite magnetic dipole orientation. As the field is applied to a particle, the subdomain with magnetization direction along the magnetic field is amplified, while the others shrink. This phenomenon is known as domain wall displacements and is shown in Figure 1.7.

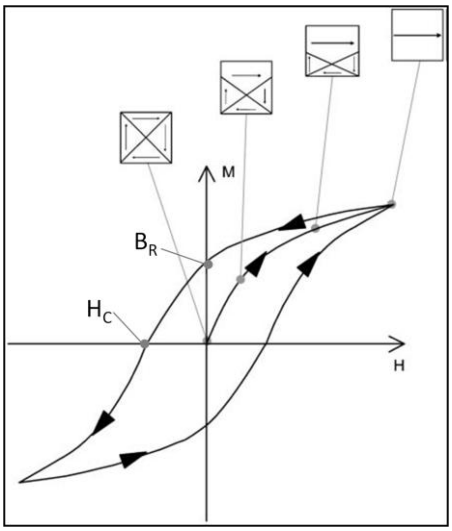

Figure 1.7: Hysteresis cycle of a multidomain magnetic material (*H* is the magnetic field amplitude, *M* is the magnetization of the material) and domain wall displacement in such a material (squares symbolize multidomain material, with magnetization of each domain; arrows on the cycle indicate the way the cycle is described when increasing or decreasing the field amplitude) [75].

Due to irreversibility of this process - magnetization curves for increasing and decreasing magnetic field amplitudes do not coincide - the material exhibits hysteresis. The energy loss due to hysteresis in an alternating magnetic field is released as heat, and can be quantified as the area within the hysteresis loop, as shown in Figure 1.7. Although several models do exist to predict hysteresis losses of ferrous particle suspensions [78-82], experimental measurements of the hysteresis loops are best because of the variability in the resultant particle magnetization.

When multidomain materials are subjected to a magnetic field, material becomes magnetic. This is shown in the hysteresis cycle when the magnetic field H is reduced to zero. This offset is known as the remanent flux density or remanence, B_R. The amount of magnetic field to cause the material to become nonmagnetic is known as coercivity, H_c. Remanence and coercivity are shown in Figure 1.7. An estimate of the amount of heating due to hysteresis losses is:

$$Q_{hyst} \approx \omega B_R H_C. \tag{1.33}$$

Hysteresis losses generally occur with large nanoparticle due to the lack of an annealing process in the nanoparticle fabrication. Annealing allows multiple grain structures to merge into one subdomain. The power losses due to Neél relaxation and hysteresis versus particle size for magnetite are shown in the following figure.

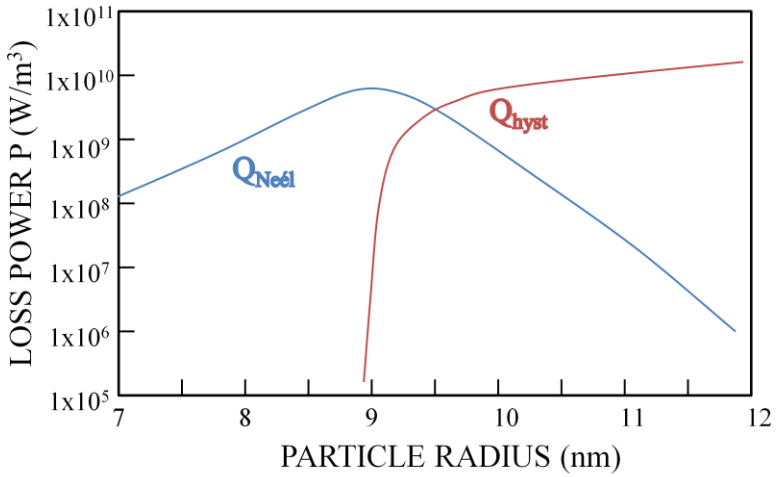

Figure 1.8: Dependence of magnetic loss power density on particle size for magnetite with a frequency of 2 MHz and field amplitude of 6.5 kA/m [75].

1.6 Organization of Thesis

The aim of the research described in this thesis is to prove that nanoparticles can enhance the efficiency of RF/microwave hyperthermia. This is shown by comparing the temperature of an inoculated region with a normal region. Temperature acquisition was accomplished by ultrasound temperature imaging. This work is documented into three chapters.

Chapter 2 describes pre-planning of ultrasound temperature imaging for RF/microwave hyperthermia therapy planning and guidance. The temperature dependence of time shifts for gelatin based phantoms, as well as porcine tissues were found. These shifts were then used to calculate the material dependent property, k, from equation (1.27) for gelatin and *ex-vivo* porcine tissue.

Chapter 3 describes RF/microwave nanoparticle absorbers. RF/microwave absorbers were selected from a broad array of different nanoparticle types. The selected nanoparticle type was then used in an *ex-vivo* study. RF/microwave therapy with the selected nanoabsorbers was monitored using ultrasound temperature imaging.

Chapter 4 summarizes the results of this work and draws conclusions. In addition, limitations and recommendations of future work are described.

1.7 References

[1] "Cancer facts and figures 2009," American Cancer Society.

[2] P. Wust, B. Hildebrandt, G. Sreenivasa, B. Rau, J. Gellermann, H. Riess, R. Felix, and P. M. Schlag, "Hyperthermia in combined treatment of cancer," *The Lancet Oncology*, vol. 3, pp. 487-497, 2002.

[3] M. R. Bailey, V. A. Khokhlova, O. A. Sapozhnikov, S. G. Kargl, and L. A. Crum, "Physical mechanisms of the therapeutic effect of ultrasound (a review)," *Acoustical Physics*, vol. 49, pp. 369-388, 2003.

[4] X. Huang, I. H. El-Sayed, W. Qian, and M. A. El-Sayed, "Cancer cell imaging and photothermal therapy in the near-infrared region by using gold nanorods," *J. Am. Chem. Soc*, vol. 128, pp. 2115-2120, 2006.

[5] C. Loo, A. Lowery, N. Halas, J. West, and R. Drezek, "Immunotargeted nanoshells for integrated cancer imaging and therapy," *Nano Letters*, vol. 5, pp. 709-712, 2005.

[6] B. Khlebtsov, V. Zharov, A. Melnikov, V. Tuchin, and N. Khlebtsov, "Optical amplification of photothermal therapy with gold nanoparticles and nanoclusters," *Nanotechnology*, vol. 17, pp. 5167-5179, 2006.

[7] X. Huang, P. K. Jain, I. H. El-Sayed, and M. A. El-Sayed, "Plasmonic photothermal therapy (PPTT) using gold nanoparticles," *Lasers in Medical Science*, vol. 23, pp. 217-228, 2008.

[8] L. R. Hirsch, R. J. Stafford, J. A. Bankson, S. R. Sershen, B. Rivera, R. E. Price, J. D. Hazle, N. J. Halas, and J. L. West, "Nanoshell-mediated near-infrared thermal therapy of tumors under magnetic resonance guidance," *Proceedings of the National Academy of Sciences*, vol. 100, pp. 13549-13554, 2003.

[9] D. M. Hall, G. R. Buettner, L. W. Oberley, L. Xu, R. D. Matthes, and C. V. Gisolfi, "Mechanisms of circulatory and intestinal barrier dysfunction during whole body hyperthermia," *American Journal of Physiology - Heart and Circulatory Physiology*, vol. 280, pp. 509-521, 2001.

[10] I. M. Germano, Y. F. Zhang, E. F. Sperber, and S. L. Moshe, "Neuronal migration disorders increase susceptibility to hyperthermia-induced seizures in developing rats," *Epilepsia*, vol. 37, pp. 902-910, 1996.

[11] B. Decadt and A. K. Siriwardena, "Radiofrequency ablation of liver tumours: systematic review," *Lancet Oncology*, vol. 5, pp. 550-560, 2004.

[12] R. Hamazoe, M. Maeta, A. Murakami, H. Yamashiro, and N. Kaibara, "Heating efficiency of radiofrequency capacitive hyperthermia for treatment of deep-seated tumors in the peritoneal cavity," *Journal of Surgical Oncology*, vol. 48, pp. 176-179, 1991.

[13] T. Livraghi, S. N. Goldberg, S. Lazzaroni, F. Meloni, T. Ierace, L. Solbiati, and G. S. Gazelle, "Hepatocellular carcinoma: radio-frequency ablation of medium and large lesions," *Radiology*, vol. 214, pp. 761-768, 2000.

[14] A. S. Wright, F. T. Lee, and D. M. Mahvi, "Hepatic microwave ablation with multiple antennae results in synergistically larger zones of coagulation necrosis," *Radiographics*, vol. 10, pp. 275-283, 2003.

[15] C. J. Simon, D. E. Dupuy, and W. W. Mayo-Smith, "Microwave ablation: principles and applications 1," *Radiographics*, vol. 25, pp. 69-83, 2005.

[16] J. Y. Shin and J. H. Oh, "The microwave absorbing phenomena of ferrite microwave absorbers," *IEEE Transactions on Magnetics*, vol. 29, pp. 3437-3439, 1993.

[17] A. N. Yusoff, M. H. Abdullah, S. H. Ahmad, S. F. Jusoh, A. A. Mansor, and S. A. A. Hamid, "Electromagnetic and absorption properties of some microwave absorbers," *Journal of Applied Physics*, vol. 92, pp. 876-882, 2002.

[18] C. L. Holloway, R. R. DeLyser, R. F. German, P. McKenna, and M. Kanda, "Comparison of electromagnetic absorber used in anechoic andsemi-anechoic chambers for emissions and immunity testing of digitaldevices," *IEEE Transactions on Electromagnetic Compatibility*, vol. 39, pp. 33-47, 1997.

[19] O. V. Salata, "Applications of nanoparticles in biology and medicine," *Journal of Nanobiotechnology*, vol. 2, pp. 3, 2004.

[20] M. Dollinger, E. H. Rosenbaum, M. Tempero, and S. J. Mulvihill, *Everyone's guide to cancer therapy: how cancer is diagnosed, treated, and managed day to day*, 4 ed: Andrews McMeel Publishing, 2002.

[21] C. C. Johnson and A. W. Guy, "Nonionizing electromagnetic wave effects in biological materials and systems," *Proceedings of the IEEE*, vol. 60, pp. 692-718, 1972.

[22] K. S. Cole and R. H. Cole, "Dispersion and absorption in dielectrics I. Alternating current characteristics," *The Journal of Chemical Physics*, vol. 9, pp. 341, 1941.

[23] A. Vorst, A. Rosen, and Y. Kotsuka, *RF/microwave interaction with biological tissues*. New York: John Wiley & Sons, 2006.

[24] Y. A. Cengel and M. A. Boles, *Thermodynamics: an engineering approach*, 4 ed. New York: McGraw Hill, 2002.

[25] H. H. Pennes, "Analysis of tissue and arterial blood temperatures in the resting human forearm," *Journal of Applied Physiology*, vol. 1, pp. 93-122, 1948.

[26] E. H. Wissler, "Pennes'1948 paper revisited," *Journal of Applied Physiology*, vol. 85, pp. 35-41, 1998.

[27] F. C. Henriques and A. R. Moritz, "Studies of thermal injury: I. the conduction of heat to and through skin and the temperatures attained therein," *Am. J. Pathol*, vol. 23, pp. 531-549, 1947.

[28] A. R. Moritz, "Studies of thermal injury: III. the pathology and pathogenesis of cutaneous burns. an experimental study*," *The American Journal of Pathology*, vol. 23, pp. 915-934, 1947.

[29] A. R. Moritz and F. C. Henriquez, "Studies of thermal iInjury: II. the relative importance of time and surface temperature in the causation of cutaneous burns," *The American Journal of Pathology*, vol. 23, pp. 693-720, 1947.

[30] J. A. Pearce, "Relationship between Arrhenius models of thermal damage and the CEM 43 thermal dose," presented at SPIE, 2009.

[31] S. A. Sapareto, *Physical aspects of hyperthermia*: American Association of Physicists in Medicine, American Institute of Physics, 1982.

[32] J. T. Beckham, M. A. Mackanos, C. Crooke, T. Takahashi, C. O'Connell-Rodwell, C. H. Contag, and E. Duco Jansen, "Assessment of cellular response to thermal laser injury through bioluminescence imaging of heat shock protein 70," *Photochemistry and photobiology*, vol. 79, pp. 76-85, 2004.

[33] R. Birngruber, *Thermal modeling in biological tissue*. New York: Plenum Press, 1980.

[34] R. Birngruber, F. Hillenkamp, and V. P. Gabel, "Theoretical investigations of laser thermal retinal injury," *Health Physics*, vol. 48, pp. 781-796, 1985.

[35] K. R. Diller, J. A. Pearce, and J. W. Valvano, "Bioheat transfer," in *The CRC Handbook of Mechanical Engineering*, F. Kreith and D. Y. Goswami, Eds.: CRC Press, 2000, pp. 4.114-4.187.

[36] S. T. Flock, L. Smith, and M. Waner, "Quantifying the effects on blood of irradiation with four different vascular-lesion lasers," presented at SPIE: Laser-Tissue Interaction IV, 1993.

[37] C. E. Fugitt, "A rate process of thermal injury," *Armed Forces Special Weapons Project AFSWP-606*, 1955.

[38] D. C. Gaylor, *Physical mechanisms of cellular injury in electrical trauma*: Massachuszetts Institute of Technology, 1989.

[39] X. He, S. McGee, J. E. Coad, F. Schmidlin, P. A. Iaizzo, D. J. Swanlund, S. Kluge, E. Rudie, and J. C. Bischof, "Investigation of the thermal and tissue injury behaviour in microwave thermal therapy using a porcine kidney model," *International Journal of Hyperthermia*, vol. 20, pp. 567-593, 2004.

[40] S. L. Jacques and M. O. Gaeeni, "Thermally induced changes in optical properties of heart," presented at IEEE Engineering in Medicine and Biology, 1989.

[41] S. L. Jacques, M. Motamedi, and S. Rastegar, "Computer simulation of laser coagulation of prostate: a guide to dosimetry. American Society for Lasers in Medicine and Surgery," *Lasers in Surgery and Medicine Suppl*, vol. 5, pp. abstract 311, 1993.

[42] S. L. Jacques and C. Newman, "Thermal coagulation of tissues: liver studies indicate a distribution of rate parameters, not a single rate parameter, describes the coagulation process," presented at Annual Winter Meeting of the American Society of Mechanical Engineers, 1991.

[43] S. L. Jacques and S. A. Prahl, "Modeling optical and thermal distributions in tissue during laser irradiation," *Lasers in Surgery and Medicine*, vol. 6, pp. 494-503, 1987.

[44] J. R. Lepock, H. E. Frey, H. Bayne, and J. Markus, "Relationship of hyperthermia-induced hemolysis of human erythrocytes to the thermal denaturation of membrane proteins," *Biochimica et Biophysica Acta*, vol. 980, pp. 191-201, 1989.

[45] D. J. Maitland and J. T. Walsh Jr, "Quantitative measurements of linear birefringence during heating of native collagen," *Lasers in Surgery and Medicine*, vol. 20, pp. 310-318, 1997.

[46] K. Matthewson, P. Coleridge-Smith, J. P. O'Sullivan, T. C. Northfield, and S. G. Brown, "Biological effects of intrahepatic neodymium: yttrium-aluminum-garnet laser photocoagulation in rats," *Gastroenterology(New York, NY. 1943)*, vol. 93, pp. 550-557, 1987.

[47] C. A. Miles, "Kinetics of collagen denaturation in mammalian lens capsules studied by differential scanning calorimetry," *International Journal of Biological Macromolecules*, vol. 15, pp. 265, 1993.

[48] N. A. Moussa, E. N. Tell, and E. G. Cravalho, "Time progression of hemolysis of erythrocyte populations exposed to supraphysiological temperatures," *Journal of Biomechanical Engineering*, vol. 101, pp. 213-217, 1979.

[49] J. A. Pearce and S. L. Thomsen, "Thermal damage parameters from laser coagulation experiments," presented at SPIE, 2003.

[50] J. A. Pearce, S. L. Thomsen, H. Vijverberg, and T. J. McMurray, "Kinetics for birefringence changes in thermally coagulated rat skin collagen," presented at SPIE, 1993.

[51] M. Pop, A. Molckovsky, L. Chin, M. C. Kolios, M. A. S. Jewett, and M. D. Sherar, "Changes in dielectric properties at 460 kHz of kidney and fat during heating: importance for radio-frequency thermal therapy," *Physics in Medicine and Biology*, vol. 48, pp. 2509-2526, 2003.

[52] M. G. Skinner, S. Everts, A. D. Reid, I. A. Vitkin, L. Lilge, and M. D. Sherar, "Changes in optical properties of ex vivo rat prostate due to heating," *Physics in Medicine and Biology*, vol. 45, pp. 1375-1386, 2000.

[53] A. N. Takata, "Development of criterion for skin burns," *Aerospace Med*, vol. 45, pp. 634-637, 1974.

[54] A. N. Takata, L. Goldfinch, J. K. Hinds, L. P. Kuan, and N. Thomopoulis, "Thermal model of laser-induced eye damage," in *Acoustical Physics*: Storming Media, 1974.

[55] A. Vassiliadis, H. C. Zweng, K. G. Dedrick, and C. Stanford Research Institute Menlo Park, "Ocular laser threshold investigations," Stanford Research Institute Menlo Park California, 1971.

[56] J. A. Weaver and A. M. Stoll, "Mathematical model of skin exposed to thermal radiation," *Aerospace Medical*, vol. 40, pp. 24-30, 1969.

[57] A. J. Welch and G. D. Polhamus, "Measurement and prediction of thermal injury in the retina of the rhesus monkey," *IEEE Transactions on Biomedical Engineering*, vol. 31, pp. 633-644, 1984.

[58] Y. C. Wu, "A modified criterion for predicting thermal injury," *National Bureau of Standards, Washington, District of Columbia*, 1982.

[59] Y. Yang, A. J. Welch, and H. G. Rylander Iii, "Rate process parameters of albumen," *Lasers in Surgery and Medicine*, vol. 11, pp. 188-190, 1991.

[60] A. J. Welch and M. J. C. v. Gemert, *Optical-thermal response of laser-irradiated tissue*. New York: Springer, 1995.

[61] N. R. Miller, J. C. Bamber, and G. R. ter Haar, "Imaging of temperature-induced echo strain: preliminary in vitro study to assess feasibility for guiding focused ultrasound surgery," *Ultrasound in Medicine & Biology*, vol. 30, pp. 345-356, 2004.

[62] C. Simon, P. VanBaren, and E. Ebbini, "Quantitative analysis and applications of non-invasive temperature estimation using diagnostic ultrasound," presented at IEEE Ultrasounics Symposium, 1997.

[63] J. Shah, S. R. Aglyamov, K. Sokolov, T. E. Milner, and S. Y. Emelianov, "Ultrasound-based thermal and elasticity imaging to assist photothermal cancer therapy - Preliminary study," presented at IEEE Ultrasonics Symposium, pp. 1029-1032, 2006.

[64] J. Shah, S. R. Aglyamov, K. Sokolov, T. E. Milner, and S. Y. Emelianov, "Ultrasound imaging to monitor photothermal therapy–Feasibility study," *Optics Express*, vol. 16, pp. 3776-3785, 2008.

[65] J. Shah, S. Park, S. Aglyamov, T. Larson, L. Ma, K. Sokolov, K. Johnston, T. Milner, and S. Emelianov, "Photoacoustic and ultrasound imaging to guide photothermal therapy: ex vivo study," presented at SPIE, vol. 6856, pp. 68560U:1-7, 2008.

[66] J. Shah, S. Thomsen, T. E. Milner, and S. Y. Emelianov, "Ultrasound guidance and monitoring of laser-based fat removal," *Lasers in Surgery and Medicine*, vol. 40, pp. 680-687, 2008.

[67] T. Varghese, J. A. Zagzebski, Q. Chen, U. Techavipoo, G. Frank, C. Johnson, A. Wright, and F. T. Lee Jr, "Ultrasound monitoring of temperature change during radiofrequency ablation: preliminary in-vivo results," *Ultrasound in Medicine & Biology*, vol. 28, pp. 321-329, 2002.

[68] R. Maas-Moreno and C. Damianou, "Noninvasive temperature estimation in tissue via ultrasound echoshifts, parts 1 and 2," *Journal of the Acoustal Society of America*, vol. 100, pp. 2514-2530, 1996.

[69] J. Shah, "Ultrasound and photoacoustic imaging to guide and monitor photothermal therapy," Ph.D dissertation, University of Texas at Austin, Austin, TX, 2008.

[70] N. P. Praetorius and T. K. Mandal, "Engineered nanoparticles in cancer therapy," *Recent Patents on Drug Delivery and Formulation*, vol. 1, pp. 37-51, 2007.

[71] C. H. Moran, S. M. Wainerdi, T. K. Cherukuri, C. Kittrell, B. J. Wiley, N. W. Nicholas, S. A. Curley, J. S. Kanzius, and P. Cherukuri, "Size-dependent joule heating of gold nanoparticles using capacitively coupled radiofrequency fields," *Nano Research*, vol. 2, pp. 400-405, 2009.

[72] J. Cardinal, J. R. Klune, E. Chory, G. Jeyabalan, J. S. Kanzius, M. Nalesnik, and D. A. Geller, "Noninvasive radiofrequency ablation of cancer targeted by gold nanoparticles," *Surgery*, vol. 144, pp. 125-132, 2008.

[73] C. J. Gannon, P. Cherukuri, B. I. Yakobson, L. Cognet, J. S. Kanzius, C. Kittrell, R. B. Weisman, M. Pasquali, H. K. Schmidt, and R. E. Smalley, "Carbon nanotube-enhanced thermal destruction of cancer cells in a noninvasive radiofrequency field," *Cancer*, vol. 110, pp. 2654-2665, 2007.

[74] R. Hergt, W. Andra, C. G. d'Ambly, I. Hilger, W. A. Kaiser, U. Richter, and H. G. Schmidt, "Physical limits of hyperthermia using magnetite fine particles," *IEEE Transactions on Magnetics*, vol. 34, pp. 3745-3754, 1998.

[75] P. P. Vaishnava, R. Tackett, A. Dixit, C. Sudakar, R. Naik, and G. Lawes, "Magnetic relaxation and dissipative heating in ferrofluids," *Journal of Applied Physics*, vol. 102, pp. 063914, 2007.

[76] A. H. Habib, C. L. Ondeck, P. Chaudhary, M. R. Bockstaller, and M. E. McHenry, "Evaluation of iron-cobalt/ferrite core-shell nanoparticles for cancer thermotherapy," *Journal of Applied Physics*, vol. 103, pp. 07A307, 2008.

[77] S. Mornet, S. Vasseur, F. Grasset, and E. Duguet, "Magnetic nanoparticle design for medical diagnosis and therapy," *Journal of Materials Chemistry*, vol. 14, pp. 2161-2175, 2004.

[78] R. Hergt, W. Andra, C. G. d'Ambly, I. Hilger, W. A. Kaiser, U. Richter, and H. G. Schmidt, "Physical limits of hyperthermia using magnetite fine particles," *IEEE Transactions on Magnetics*, vol. 34, pp. 3745-3754, 1998.

[79] D. C. F. Chan, D. B. Kirpotin, and P. A. Bunn, "Synthesis and evaluation of colloidal magnetic iron oxides for the site-specific radiofrequency-induced hyperthermia of cancer," *Journal of Magnetism and Magnetic Materials*, vol. 122, pp. 374-378, 1993.

[80] A. Jordan, P. Wust, H. Fähling, W. John, A. Hinz, and R. Felix, "Inductive heating of ferrimagnetic particles and magnetic fluids: physical evaluation of their potential for hyperthermia," *International Journal of Hyperthermia*, vol. 9, pp. 51-68, 1993.

[81] E. Kneller, *Theory of the magnetization curve of small crystals*, vol. 18, 2 ed. New York: Springer-Verlag, 1966.

[82] S. Chikazumi, *Physics of Magnetism*. Philadelphia, PA: Lippincott, 1964.

Chapter 2: Ultrasound Temperature Monitoring

2.1 Introduction

Several ultrasound methods have been proposed to estimate temperature, such as monitoring attenuation [1], backscattered power [2], and propagation speed [3]. Thermal expansion has also been investigated in conjunction with propagation speed; however, between 37˚C and 60˚C the propagation speed dependency in ultrasound imaging with temperature is far more significant when compared to thermal expansion [4]. In addition, attenuation and backscattered power dependencies on temperature are far less significant than the propagation speed. Most of the underlying fundamentals of propagation speed temperature tracking with ultrasound were covered in Section 1.4 of Chapter 1.

Notice that equation (1.27) $\left(\Delta T = k\frac{d(\Delta t)}{dt}\right)$ has a material dependent quantity. This quantity describes the dependence of the speed of sound with temperature, as shown in equation (1.26) $\left(\Delta t = 2z\left[\frac{1}{c(T_0+\Delta T)} - \frac{1}{c(T_0)}\right]\right)$. The speed of sound in defined by the following relationship:

$$c(T) = \sqrt{\frac{B(T)}{\rho(T)}}, \tag{2.1}$$

where B is the bulk modulus of the medium and ρ is the density of the medium. Tables of the bulk modulus and density versus temperature are widely available in material property references for several materials. For example, using the volume properties of

water from the CRC Handbook of Chemistry and Physics [5], the following curves are generated for the speed of sound, density, and bulk modulus versus temperature.

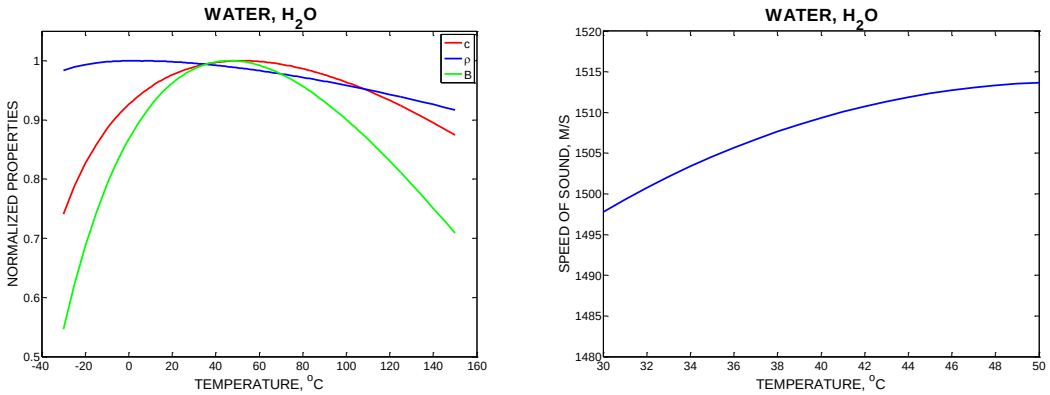

Figure 2.1: Normalized speed of sound (c), density (ρ), and bulk modulus (B) on the left; speed of sound on right; values of water taken from [5].

Most tissues of the body have a speed of sound that behaves in the same pattern as water (Figure 2.2). However, fat has low water content compared to other tissues and the speed of sound behaves as shown in Figure 2.3.

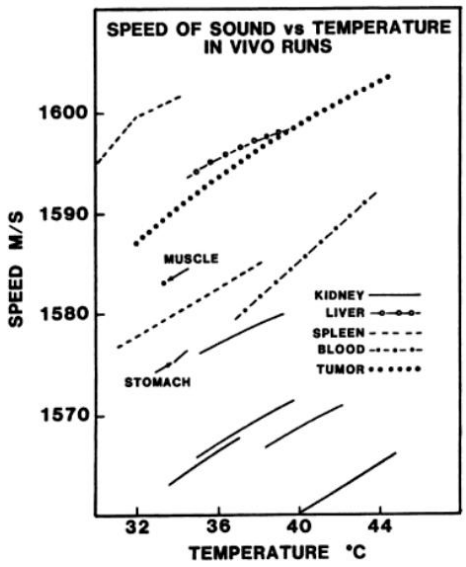

Figure 2.2: Speed of sound versus temperature for various tissues [6].

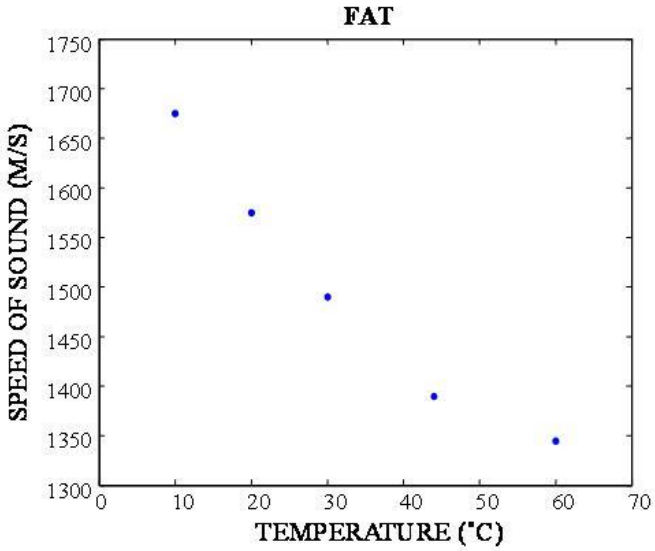

Figure 2.3: Speed of sound versus temperature for peritoneal fat taken from [7].

This chapter gives experimentally acquired k values for gelatin phantoms and *ex-vivo* porcine tissues. Phantoms were made from porcine gelatin that closely mimic water-based tissues. In addition, the *ex-vivo* porcine muscle and porcine fat were studied. Ultrasound imaging frames were acquired every 0.5˚C increase for each sample. The material dependent k values were calculated from temperature changes within the 15˚C to 25˚C temperature range. The assumption of linearity of the k value with temperature provides an accurate normalized time shift correlation to differential temperature as long as physical motion can be compensated [5].

2.2 Materials and Methods

2.2.1 Sample Preparation

Experiments were first performed using 50 mm by 50 mm by 100 mm tissue mimicking phantoms constructed from porcine gelatin. Gelatin has high water content

which is representative of the RF/microwave electromagnetic energy losses in many tissues. The gelatin phantoms were fabricated using 8% by weight aqueous solution of porcine gelatin (Sigma-Aldrich, USA). This aqueous solution also contained 0.4% by weight 40 μm silica particles. These particles behave as ultrasound scatterers; thus, enabling speckle tracking during ultrasound temperature imaging. The aqueous gelatin solution was poured into an appropriate mold and was allowed to solidify in a 2˚C refrigerator for about 30 minutes. *Ex-vivo* studies were performed using fresh porcine *longissimus dorsi* muscle and porcine fat. The samples were 50 mm by 50 mm by 100 mm and B-mode ultrasound images are shown in Figure 2.4 for gelatin, porcine muscle, and porcine fat.

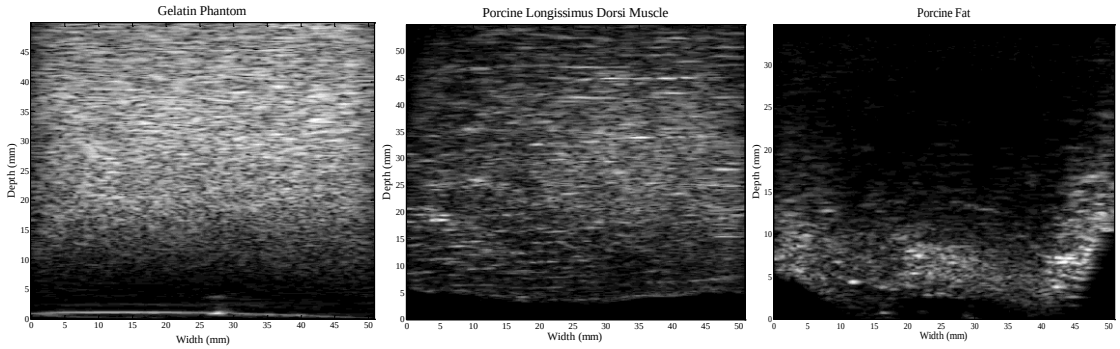

Figure 2.4: B-mode images of 8% porcine gelatin (left), porcine *longissimus dorsi* muscle (center), and porcine fat (right). The transducer is located at the at 0 mm of depth on the images. Notice that the B-mode image of porcine fat is highly attenuating.

2.2.2 Experimental Setup

The experimental setup for the determination of the material dependent property, k, is shown in Figure 2.5. This setup utilizes a Sonix RP imaging system (Ultrasonix Medical Corporation, Burnaby, Canada) equipped with a 128 element linear

array transducer operating at a 5 MHz center frequency. The reference temperature measurement was performed with a type-K thermocouple (Thermoworks, Alpine, UT). The sample was immersed in a temperature regulating water bath (Isotemp 3013H, Fisher Scientific, Pittsburg, PA).

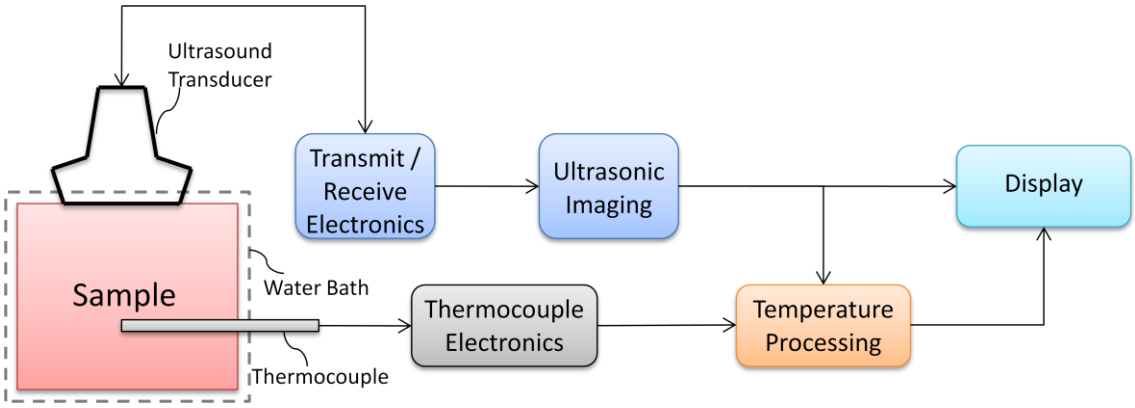

Figure 2.5: Experimental setup for ultrasound time shifts versus temperature.

The sample temperature was increased from 15˚C to 25˚C with ultrasound frames captured every 0.5˚C. The temperature distribution within each ultrasound frame was assumed to be spatially homogeneous. A 10 mm by 10 mm region near the thermocouple was used to determine the normalized time shift. The speckle pattern from each successive ultrasound frame was correlated to the first acquired frame temporally. The spatial gradients of the time shifts were then computed. These apparent time shifts were then used to find the material dependent property, k.

2.3 Results

Due to the ~30°C melting point of the aqueous 8% porcine gelatin by weight, the ultrasound B-mode imaging frames were acquired between 15°C and 25°C for the gelatin, porcine muscle, and porcine fat. In addition, regions within the images were selected with the highest correlation. Figures 2.6 through 2.8 depict the apparent time shifts versus depth for temperatures between 15°C and 25°C.

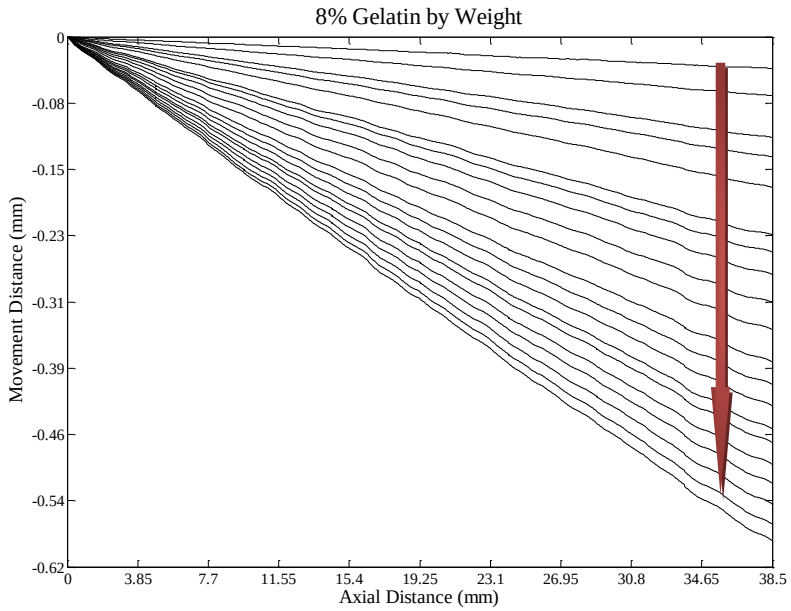

Figure 2.6: Apparent time shifts for 8% gelatin with red arrow indicating increase in differential temperature. The temperature was increased from 15˚C to 25˚C in 0.5˚C increments.

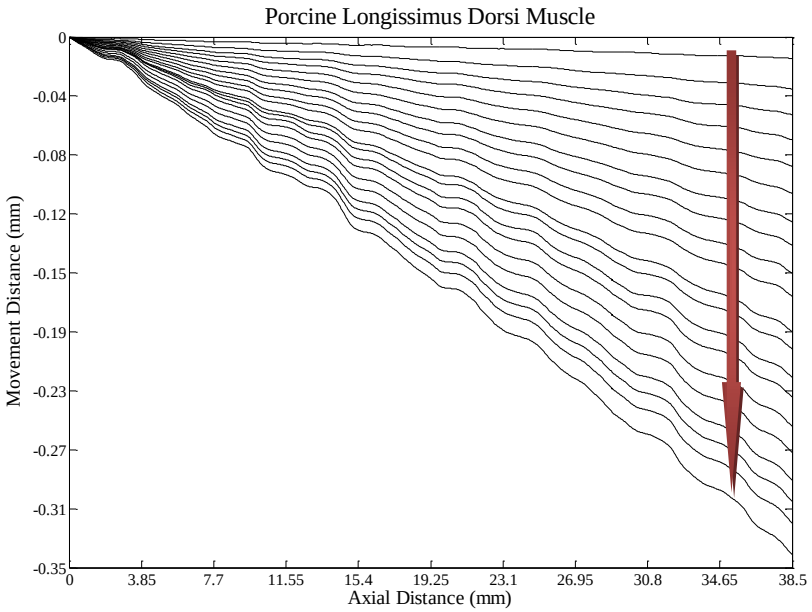

Figure 2.7: Apparent time shifts for porcine *longissimus dorsi* muscle with red arrow indicating increase in differential temperature. The temperature was increased from 15˚C to 25˚C in 0.5˚C increments. Notice that the movement distance decreases with temperature in gelatin and porcine muscle.

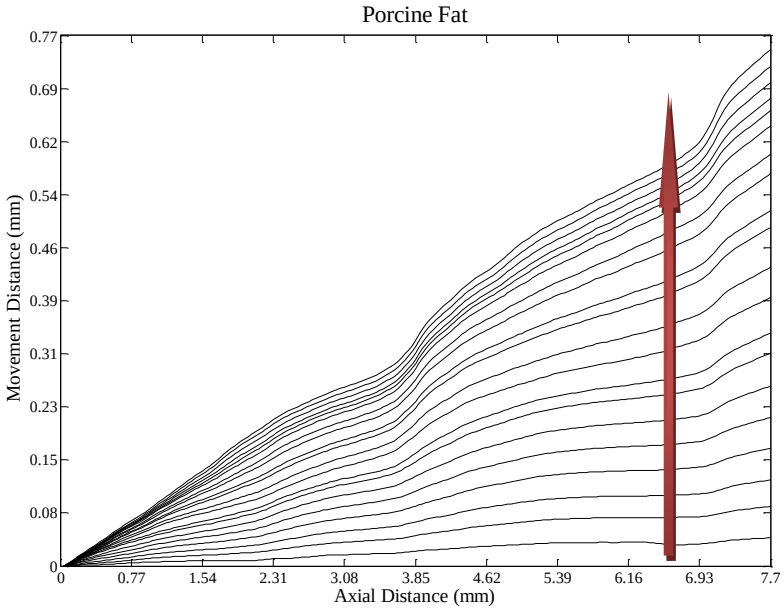

Figure 2.8: Apparent time shifts for porcine fat with red arrow indicating increase in differential temperature. The temperature was increased from 15˚C to 25˚C in 0.5˚C increments. Notice that the movement distance increases with temperature unlike the gelatin and porcine muscle.

Notice that the apparent time shifts (y-axis) increase with axial distance due to the accumulation of shift, as shown in equation (1.26). The dependence on depth was removed by taking the spatial gradient (spatial normalization). Final correlation of the time shifts utilizes a medium dependent property, k, to characterize the trend of the differential temperature versus different normalized time shifts. The k value is the slope of a least squares regression line with a forced intercept value of zero of the normalized time shift versus temperature, as shown in the Figures 2.9-2.11.

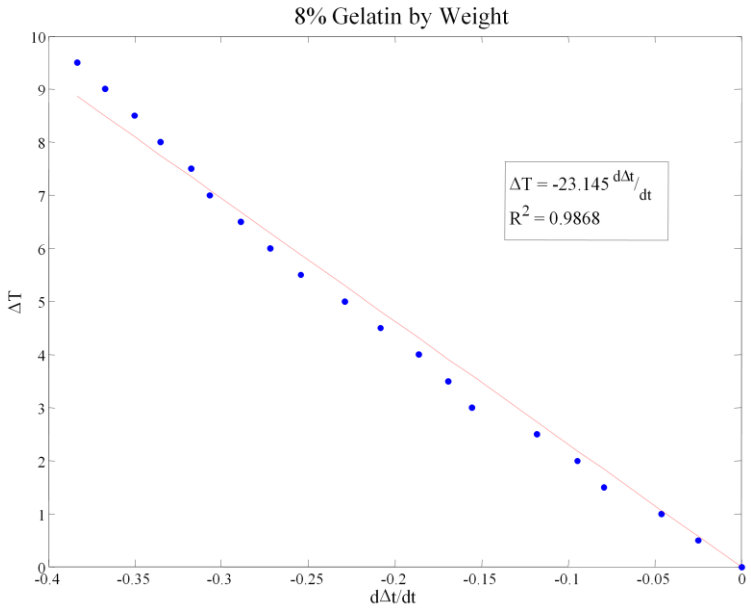

Figure 2.9: Differential temperature versus apparent time shift. Circles are the values of the normalized time shifts; red line is regression line; k value is -23.1.

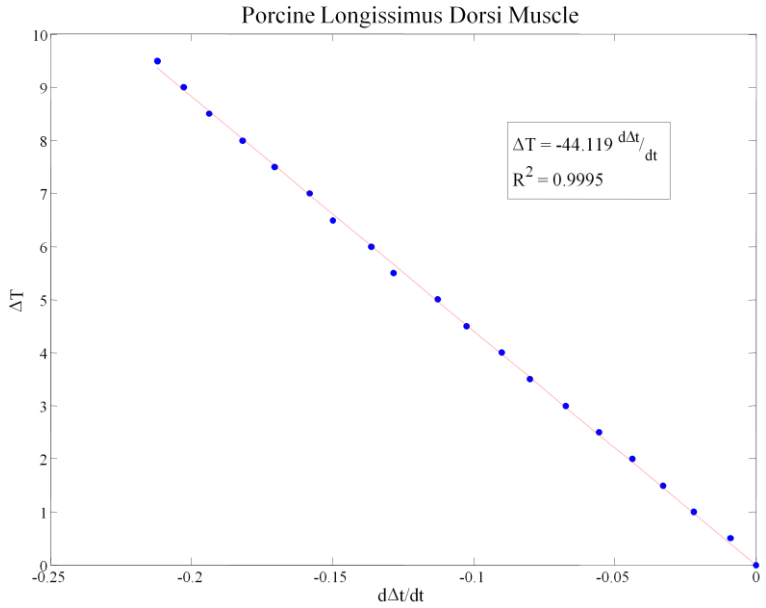

Figure 2.10: Differential temperature versus apparent time shift. Circles are the values of the normalized time shifts; red line is regression line; k value is -44.1.

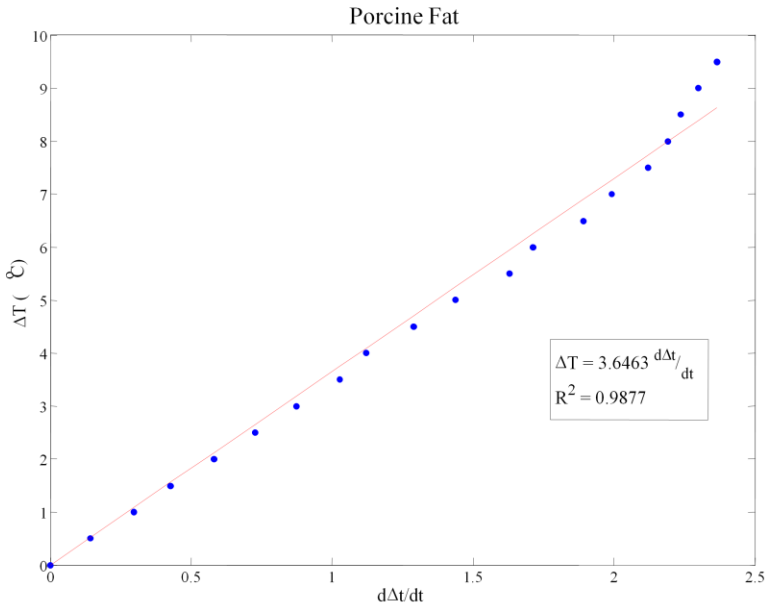

Figure 2.11: Differential temperature versus apparent time shift. Circles are the values of the normalized time shifts; red line is regression line; k value is +3.6.

2.4 Discussion

The gelatin phantom represents the ideal case because the medium is homogeneous with respect to the speed of sound. This is illustrated in the smooth lines presented in Figure 2.6. Porcine muscle is a more realistic case in that the medium is heterogeneous. Muscles contain some fat deposits, connective tissues, and vessels. Therefore, k values are no longer tissue type-specific, but tissue-location specific. The heterogeneity of porcine muscle is demonstrated in Figure 2.7 with the nonlinear apparent time shift lines.

The assumption that the differential temperature versus normalized time shifts curve is linear is somewhat inaccurate for tissues, as shown in Figure 2.12. The increase in muscle tissue temperatures induces reversible collagen shrinkage. Collagen shrinkage is thought to occur when hydrothermal agitation is sufficient to overcome the forces, chiefly hydrogen bonds, which hold together the polypeptide chains [8]. Without the separating forces induced by hydrogen bonds, the polypeptide chains in collagen collapse. Therefore, collagen shrinkage causes the physical shrinkage and an increase in the bulk modulus of tissues [9,10]. The physical shrinkage and increase in bulk modulus will cause increased apparent time shifts, which may not be linear, as shown in Figure 2.12. This is due to the nonlinearity of collagen shrinkage with temperature.

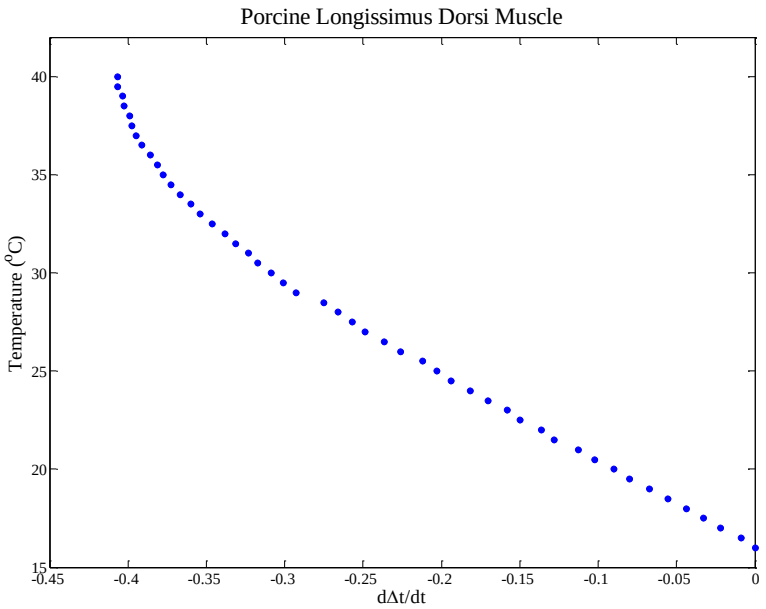

Figure 2.12: Differential temperature versus apparent time shift for porcine muscle. Circles are the values of the normalized time shifts. Temperatures were acquired between 16˚C and 41˚C.

Notice that the speed of sound in gelatin and porcine muscle increases with temperature (Figures 2.9 and 2.10). On the other hand, the speed of sound in porcine fat decreases with increasing temperature (Figure 2.11). This is primarily due to the trend of the bulk modulus, which is inversely proportional to the compressibility. In gelatin and muscle, the compressibility decreases with increasing temperature because of protein collapse [8]. Fat molecules at low temperature are more susceptible to link via van der Waals interactions. As the temperature increases, the van der Waals are weakened due to an increase in molecular kinetic energy, thus increasing the compressibility of fat. Therefore, the inverse proportionality of the speed of sound with temperature is expected in porcine fat.

2.5 Summary

Correlation values of differential temperature to normalized time shifts were found for 8% gelatin by weight, porcine *longissimus dorsi* muscle, and porcine fat. Ultrasound images were gathered in 0.5˚C intervals for determination of the correlation values. At certain temperature collagen shrinkage affects the curvature of the differential temperature versus normalized time shift curve for muscle. Fats exhibit apparent time expansion with increasing temperature, whereas gelatin and muscle exhibit apparent time shrinkage. By accounting for this curvature with realistic k value determinations, accurate differential temperature images can be acquired.

2.6 References

[1] S. Ueno, M. Hashimoto, H. Fukukita, and T. Yano, "Ultrasound thermometry in hyperthermia," presented at IEEE Ultrasonics Symposium, 1990.

[2] W. L. Straube and R. M. Arthur, "Theoretical estimation of the temperature dependence of backscattered ultrasonic power for noninvasive thermometry," *Ultrasound in Medicine & Biology*, vol. 20, pp. 915-922, 1994.

[3] R. L. Nasoni, "Temperature corrected speed of sound for use in soft tissue imaging," *Medical Physics*, vol. 8, pp. 513-515, 1981.

[4] T. Varghese, J. A. Zagzebski, Q. Chen, U. Techavipoo, G. Frank, C. Johnson, A. Wright, and F. T. Lee Jr, "Ultrasound monitoring of temperature change during radiofrequency ablation: preliminary in-vivo results," *Ultrasound in Medicine & Biology*, vol. 28, pp. 321-329, 2002.

[5] C. R. Company, *CRC handbook of chemistry and physics*, 69 ed. Boca Raton, Florida: CRC Press, Inc., 1988.

[6] S. Mizushina, *Non-invasive temperature measurement*: Gordan and Breach Science Publishers, 1988.

[7] B. Rajagopalan, J. F. Greenleaf, P. J. Thomas, S. A. Johnson, and R. C. Bahn, "Variation of acoustic speed with temperature in various excised human tissues studied by ultrasound computerized tomography," *Ultrasonic tissue characterization II. National Bureau of Standards, Washington DC*, pp. 227-233, 1979.

[8] P. C. Brown, R. Consden, and L. E. Glynn, "Observations on the Shrink Temperature of Collagen and its Variations with Age and Disease," *British Medical Journal*, vol. 17, pp. 196, 1958.

[9] R. Brinkmann, B. Radt, C. Flamm, J. Kampmeier, N. Koop, and R. Birngruber, "Influence of temperature and time on thermally induced forces in corneal collagen and the effect on laser thermokeratoplasty," *Journal of Cataract & Refractive Surgery*, vol. 26, pp. 744-754, 2000.

[10] C. T. Vangsness, W. Mitchell, M. Nimni, M. Erlich, V. Saadat, and H. Schmotzer, "Collagen shortening," *Clin Orthop*, vol. 337, pp. 267-71, 1997.

Chapter 3: Microwave Absorbing Nanoparticles and Therapy

3.1 Introduction

RF/microwave cancer hyperthermia using nanoparticles has been under study as early as 1957. Gilchrist et al. attempted to heat various tissue samples using the heat dissipated from 20 to 100 nm nanoparticles of maghemite (γ-Fe_2O_3) exposed to an alternating magnetic field of 1.2 MHz [1]. Although there was localized heating in the region of interest, biocompatibility and targeting problems of the nanoparticles and insufficient energy applicators placed constraints on the viability of their use in clinical applications. Throughout the late 1970s and early 1980s immense amounts of cancer research efforts were devoted to RF/microwave hyperthermia. Technological advances here enabled for electromagnetic power deliver to deep lying structures; however, nanoparticle targeting was still an issue. Current advances in surface modification of nanoparticles have enabled targeting of several cancer types [2-4]. To date, investigators have utilized stablilzed nanoparticles for radiofrequency therapy at frequencies of 100 kHz, 150 kHz, and 13.56 MHz [5-15].

One method to induce hyperthermia with nanoparticles is to capacitively couple the nanoparticle to an alternating electric field. This is most commonly accomplished with parallel plate transceivers. An alternating voltage potential is placed across the plates with the region of interest is placed between the plates. A system that several investigators use is the one proposed by John Kanzius [16-20]. This system delivers a 13.56 MHz alternating voltage potential across a region of interest. This system has

been shown to be effective with gold nanospheres and carbon nanotubes. Several investigator claims that the primary mechanism responsible for heating is joule heating of the nanoparticle [6-7]. However, the particles induce Joule heating of the tissue directly around the particle due to 'focusing' of the electromagnetic field, as shown in Section 1.5.1 of Chapter 1.

The other method to induce hyperthermia with nanoparticles is with an alternating magnetic field. Alternating magnetic fields are usually accomplished by placing objects within an inductive coil; however, the field is concentrated close to the coil which is usually away from the region of interest. A system that is used by Magforce (Berlin, Germany) utilizes a magnetic circuit, as shown in Figure 3.1. The current carrying wire induces a magnetic flux, Φ, in the magnetic conductor. Because it is a series magnetic circuit, the magnetic flux in the magnetic material is equal to the magnetic flux in the gap. Within this gap is where the tissue is placed. The nanoparticle behavior in an alternating magnetic field is clearly described in Section 1.5.2 of Chapter 1.

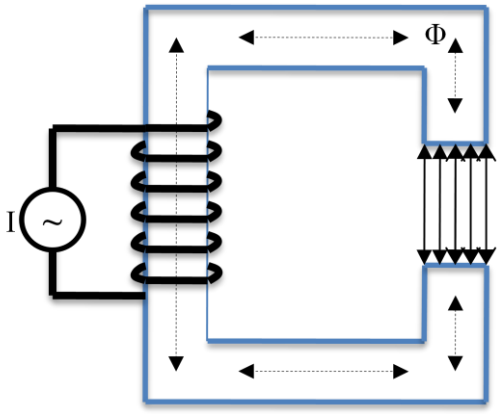

Figure 3.1: Magnetic circuit with gap for therapeutic delivery; I is the alternating current and Φ is the magnetic flux [8].

One method that has not been explored in conjunction with nanoparticles is high radio frequencies, or microwaves. A major advantage of using microwaves is the ability to make compact applicators. Another advantage is the ability to quickly deposit energy in the nanoparticles. Microwave ablation has been utilized in the clinical setting with hepatic lesions, as well as in the prostate [21,22]. Since microwave emission is electric field dominant, the dominant mode of heating is joule heating from eddy currents that develop in the conducting particles. The eddy current layer becomes smaller with increasing frequency because of the skin effect, given by:

$$\delta = \sqrt{\frac{1}{\pi f \sigma |\mu^*|}}, \tag{3.1}$$

where δ is the skin depth, σ is the electrical conductivity of the particle, f is the frequency of the source, and $|\mu^*|$ is the absolute magnetic permeability. Joule heating is proportional to resistance for a given potential, and resistance is given by:

$$R = \frac{l}{\sigma A}, \tag{3.2}$$

where l is the length and A is the cross-sectional area of the conductor. Therefore, the resistance increases with frequency due to a decrease in cross-sectional area due to the skin effect, thus an increase in Joule heating.

This chapter details experimental outcomes of using microwaves at 2.45 GHz in conjunction with microwave absorbing nanoparticles. First, several nanoparticles were acquired to determine the relative absorption of energy. Secondly, differential temperature maps were calculated for *ex-vivo* porcine tissues with nanoparticle inclusions. The results give evidence for clinical viability of microwave hyperthermia for superficial treatment.

3.2 Materials and Methods

3.2.1 Nanoparticle Selection

Experiments were performed using 8 cm by 8 cm by 2 cm blocks of polyvinyl alcohol (PVA) with 7 cylindrical holes for PVA/nanoparticle mixtures. These blocks were constructed by mixing 8% PVA (Celanese Celvol 165SF, Dallas, TX) by weight with water. The mixture was then poured into a mold followed by freezing the mixture for 12 hours at ~ -5°C then thawed at ~ 20°C for 12 hours [23]. The freeze-thaw cycle was repeated for another 3 cycles. PVA was selected because ease of manufacture with minimal entrained air. In addition, PVA has low thermal conductivity, thus allowing for minimal thermal diffusion.

Six nanoparticle types were selected because of their behavior in response to electromagnetic fields. Gold and silver nanoparticles were selected because of their

high electrical conductivity. Graphite was selected because of the successful heating with carbon nanotubes at 13.56 MHz [7]. Cobalt and iron-oxide were selected because of their high magnetization. The final nanoparticle list included: 20 nm thick nanoshell over a 20 nm maghemite (γ-Fe_2O_3) core [24], densely packed silver nanocages over a 520 nm silica core [25], loosely packed silver nanocages over a 520 nm silica core [25], 20 nm maghemite (γ-Fe_2O_3) nanospheres [24], 20 nm carbon coated cobalt (Nanoamor, Houston, TX), and 1-100 µm graphite flakes (Dixon, Asbury, NJ). The seventh hole was left void to display the "edge effect heating" caused by incident electromagnetic energy entering multiple surfaces. The nanoparticles were mixed with 8% PVA by weight with water. The concentration of the nanoparticles was 74.9 µg per milliliter of aqueous PVA. The phantom then experienced two freeze-thaw cycles, as described above. The final configuration of the PVA block is shown in the following figure.

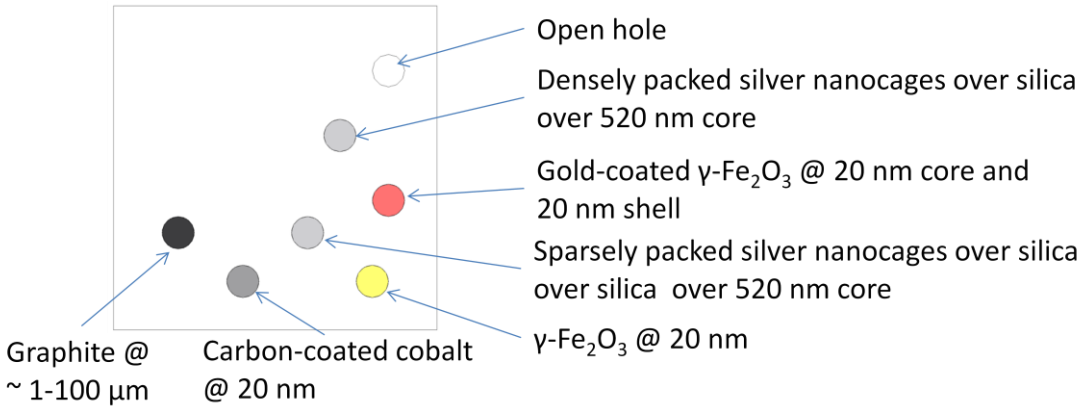

Figure 3.2: Configuration of PVA block for microwave energy to heat conversion for 6 different types of nanoparticle.

3.2.1.1 Experimental Setup

This experiment utilizes a 90° corner reflecting microwave antenna emitting a 2.45 GHz 100 W microwave placed 3 cm from the surface of the PVA block for 10 minutes. After exposure, an Inframetric Model 525 infrared scanning radiometer (Inframetrics, Bedford, MA) captured the thermal map of the PVA block surface. The configuration of the thermal image is shown in Figure 3.3

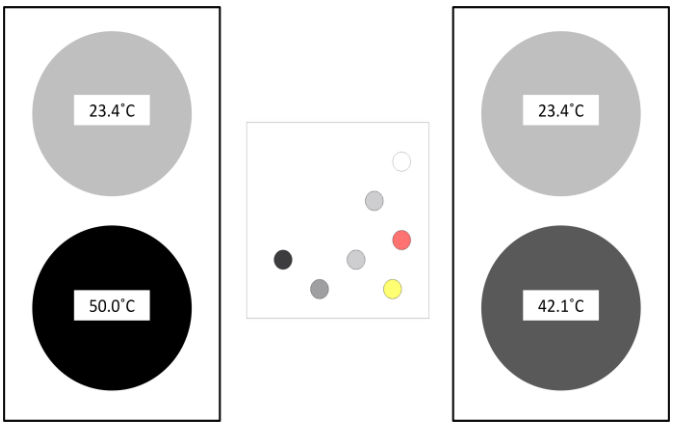

Figure 3.3: Configuration of PVA block for microwave energy to heat conversion with black bodies to calibrate thermal map.

The black bodies were set at 23.4˚C, 42.1˚C, and 50.0˚C. These temperatures were used in the thermal image to correlate the captured infrared intensity with temperature.

The correlation of temperature to emission power is given by Planck's law of black body radiation:

$$W_b(\lambda, T) = \frac{2\pi hc^2}{\lambda^5\left(e^{\frac{hc}{\lambda k_b T}} - 1\right)}, \tag{3.3}$$

where W_b is the surface monochromatic emissive power, h is Planck's constant ($6.627x10^{-34}Js$), c is the speed of light, λ is the wavelength, and k_b is the Boltzmann constant ($1.381x10^{-23}J/K$). Notice that this relationship accounts for only monochromatic emissions. Since the Inframetrics Model 525 operates in the 8 to 12 μm band, the following relationship must be used [26]:

$$E_b(T) = \int_{\lambda_1}^{\lambda_2} W_b(\lambda, T)d\lambda. \quad (3.4)$$

These relationships accounts for ideal black bodies; however, PVA, and tissues, are gray bodies. Gray bodies can be accounted for by a property called "emissivity" which is the effective radiation efficiency. The following relationship accounts for the loss of efficiency assuming uniform temperature within the region of interest.

$$E_b(T_{roi}) = \frac{E_b(T)-(1-\varepsilon)E_b(T_{amb})}{\varepsilon}. \quad (3.5)$$

where T_{roi} is the temperature at the region of interest, T_{amb} is the ambient temperature, and ε is the emissivity (assumed to be 0.95 for PVA).

The thermal map was computed by finding calibrating the image intensity from the black bodies. This was done by inserting the black body temperatures into equation (3.4). Then appropriate scaling of the image intensity was performed. Equation (3.5) was used to calculate the temperatures across the surface of the PVA block.

3.2.2 *Ex-vivo* Studies

Experiments were performed with excised *longissimus dorsi* porcine tissue. Injections of a mixture of 0.1 ml of 20-50 nm magnetite with 100 ml of water was

distributed within a small portion of the porcine tissue. The configuration of this injection is shown in Figure 3.4.

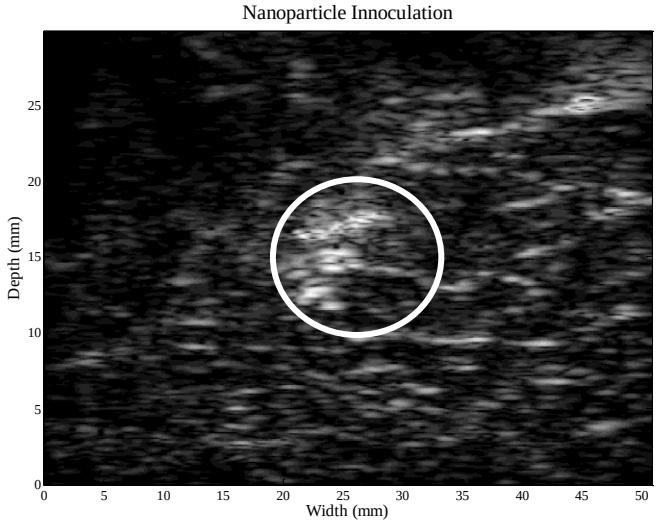

Figure 3.4: B-mode image of the porcine *longissimus dorsi* muscle after nanoparticle inoculation with the white circle displaying area of innoculation.

3.2.1.1 Experimental Setup

This experiment involves heating the *ex-vivo* tissue with a 2.45 GHz microwave for 1 minute. The microwave incident power was set to 130 W. The thermal map was gathered through ultrasound thermal imaging. The ultrasound frames were captured using the Sonix RP imaging system (Ultrasonix Medical Corporation, Burnaby, Canada) equipped with a 128 element linear array transducer operating at a 5 MHz center frequency. The frames were captured every 10 seconds during the microwave treatment. The differential temperatures were calculated by multiplying the normalized

time shifts with the material dependent property, k, found in chapter 3 for porcine muscle. The experimental setup is shown in Figure 3.5.

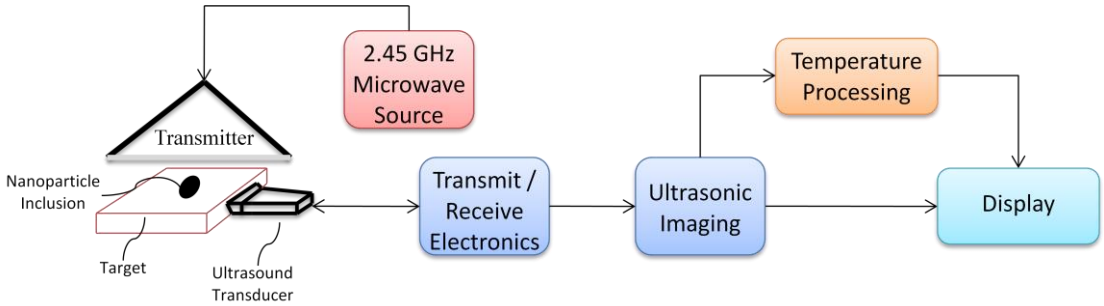

Figure 3.5: Microwave hyperthermia system with ultrasound temperature monitoring system.

3.3 Results

3.3.1 Nanoparticle Selection

The initial image from the infrared radiometer is shown in Figure 3.6. The blackbody to the upper right corner is 24.1°C and the intensity value acquired from the thermal radiometer was ~85.

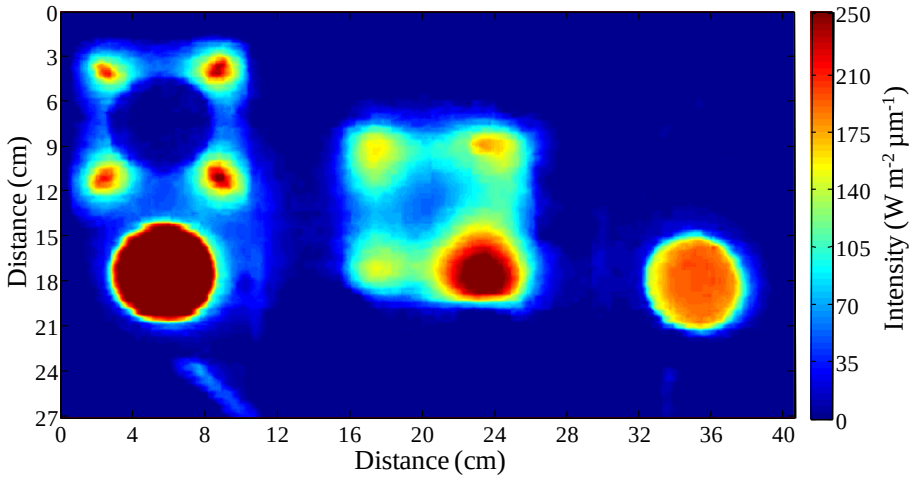

Figure 3.6: Thermal image of PVA block with 6 different nanoparticles with black bodies to calibrate image intensity. Image was acquired after 10 minutes of microwave exposure at 100W.

Using equations (3.3) and (3.4), the intensity power should be ~115. Therefore, scaling the image was necessary to attain an accurate thermal image. After scaling the image intensities to emission powers and accounting for a 0.95 emissivity, the following temperature map was generated:

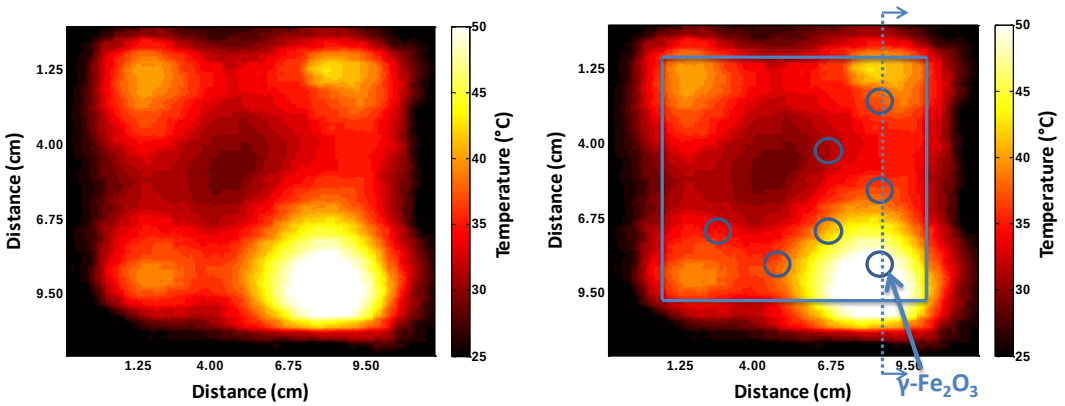

Figure 3.7: Temperature profile of PVA block after 10 minute microwave exposure at 100W.

As displayed in Figure 3.7, the maghemite had more energy release in the form of heat. The temperature distribution across a line, as shown in Figure 3.8, demonstrates a large differential temperature of the maghemite region.

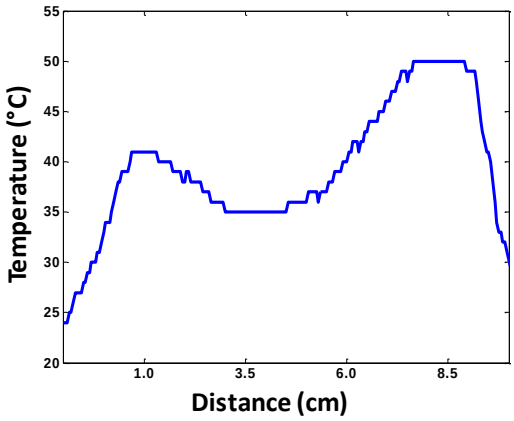

Figure 3.8: Temperature distribution from cross-section illustrated in Figure 3.7.

Also notice the high differential temperatures focused on the edges of the phantom. This was due to the microwaves penetrating multiple surfaces; thus, causing a large volumetric power distribution within these regions. Therefore, more dielectric heating occurs within the PVA around the edges and corners.

3.3.2 *Ex-vivo* Studies

The ultrasound image of the *ex-vivo* porcine *longissimus dorsi* muscle is presented in the upper left of Figure 3.9. The thermal images of the tissue recorded during 10, 20, 30, 40, and 50 seconds of 2.45 GHz microwave irradiation at 100 W are shown in Figure 3.9.

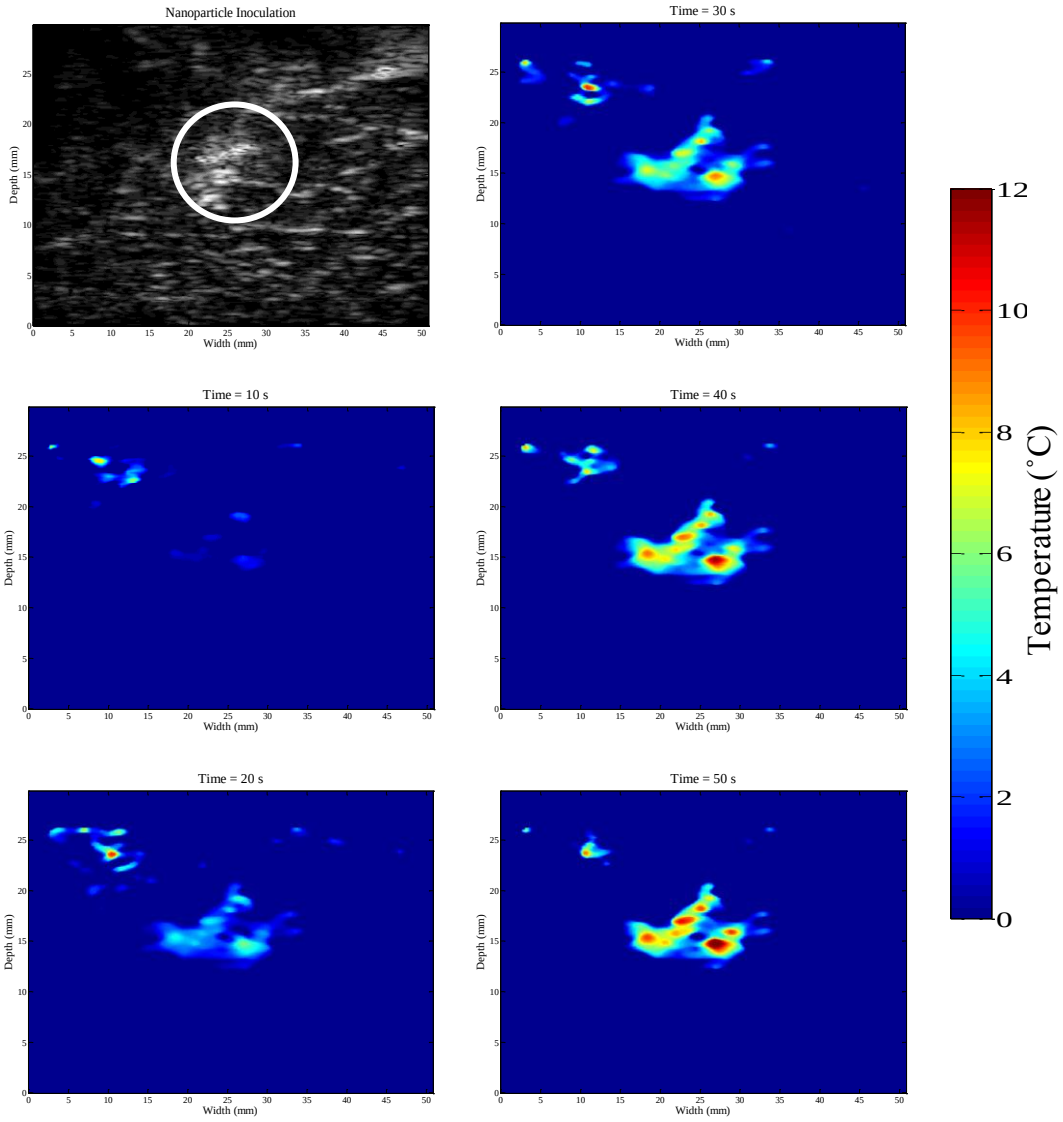

Figure 3.9: Ultrasound temperature images of porcine *longissimus dorsi* muscle tissue with nanoparticle inoculation. Images acquired at 10 s, 20 s, 30 s, 40 s, and 50 s.

The area with magnetite nanoparticle inoculations is shown by the white circle overlaying the grayscale B-mode ultrasound image. Data obtained from the water bath experiments, Figure 2.10, were used to convert the normalized time shifts from the captured ultrasound frame to temperature. This was adequate because the initial

temperature of the tissue was 15˚C. The thermal maps in Figure 3.9 show a progressive increase in temperature with irradiation time. The images were scaled so that the tissue surrounding the inoculation site had a differential temperature of ~0˚C. A curve showing the average differential temperature versus time for a 1 mm by 1 mm area within the magnetite inoculation is shown in Figure 3.10.

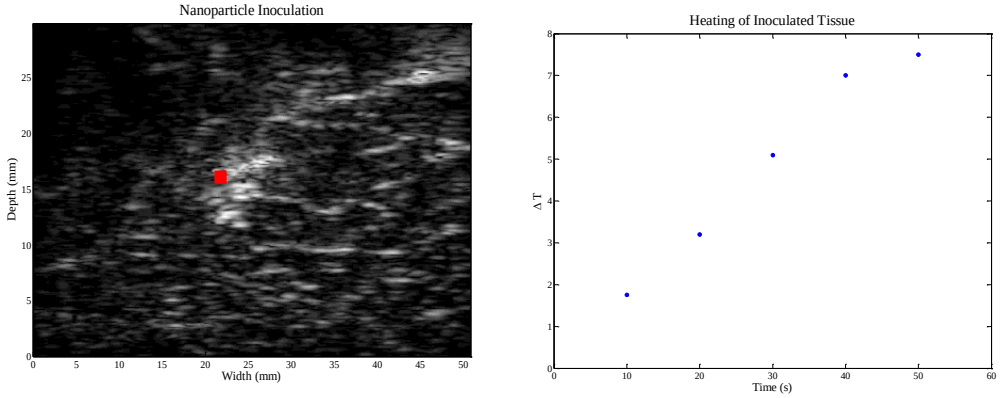

Figure 3.10: Differential temperature of a 1 mm by 1 mm region (shown in red on left) versus treatment time.

3.4 Discussion

Due to the nature of the microwave emission, the radiated power is electric field dominated; therefore, the majority of heating is electric field heating. Since the nanoparticle selection experiment maintained approximately the same heat capacity, volume, and electric field, the number of particles played the deciding factor of heating. This is due to the fact that the gold and silver particles should produce more heat because they have larger electrical conductivities and should have more concentrated electric fields directly around the particles. In addition, the effective particle volumes of the gold coated maghemite and silver nanocages were larger. However, due to the

much higher density of gold (19.3 g/cc) in comparison to maghemite (4.9 g/cc) and the size of the silver nanocages, the number of particles was far less because the standardization of the nanoparticles in the inclusions to weight. The phantom and *ex-vivo* studies were carried out by iron-oxide; however, experiments that standardize the particles by number or volume should be explored. Magnetite is very similar in electrical and physical properties to maghemite, and has the added benefit of being FDA approved. Thus, *ex-vivo* studies were conducted using magnetite since there was availability at 20 nm.

As shown in Figure 3.9, a small area outside the inoculation region displays a temperature increase. This is an artifact due to low imaging signal in that region. The lack of signal leads to inaccurate speckle tracking, thus inaccurate time shift calculations. This can be compensated by masking the ultrasound thermal maps in areas with low ultrasound speckle. Other miscalculations of temperature arise from tissue inhomogeneity in the porcine *longissimus dorsi* muscle due to numerous fat deposits. This is due to the difference in the k value for porcine fat. However, Figure 3.9 doesn't display any significant temperature inaccuracies from heterogeneity of the tissue.

3.5 Summary

Results of this chapter suggest that 20 nm magnetite is a good absorber of 2.45 GHz microwave energy. Targeting these nanoparticles can lead to noninvasively inducing large differential temperature within a selected tissue. Higher concentrations

of gold and silver nanoparticles should be considered because of their high electrical conductivity. Porcine *longissimus dorsi* muscle heterogeneity didn't affect the ultrasound temperature image; however, insufficient signal due to a lack of ultrasound scatterers induced artifacts in the temperature images. Overall, microwave absorbing nanoparticles increase the efficiency in microwave hyperthermia of selected tissues.

3.6 References

[1] R. K. Gilchrist, R. Medal, W. D. Shorey, R. C. Hanselman, J. C. Parrott, and C. B. Taylor, "Selective inductive heating of lymph nodes," *Annals of Surgery*, vol. 146, pp. 596-606, 1957.

[2] X. Gao, Y. Cui, R. M. Levenson, L. W. K. Chung, and S. Nie, "In vivo cancer targeting and imaging with semiconductor quantum dots," *Nature Biotechnology*, vol. 22, pp. 969-976, 2004.

[3] O. C. Farokhzad, S. Jon, A. Khademhosseini, T. N. T. Tran, D. A. LaVan, and R. Langer, "Nanoparticle-Aptamer Bioconjugates A New Approach for Targeting Prostate Cancer Cells," vol. 64: AACR, 2004, pp. 7668-7672.

[4] O. C. Farokhzad, J. M. Karp, and R. Langer, "Nanoparticle-aptamer bioconjugates for cancer targeting," *Expert Opin. Drug Deliv.*, vol. 3, pp. 311-324, 2006.

[5] C. H. Moran, S. M. Wainerdi, T. K. Cherukuri, C. Kittrell, B. J. Wiley, N. W. Nicholas, S. A. Curley, J. S. Kanzius, and P. Cherukuri, "Size-dependent joule heating of gold nanoparticles using capacitively coupled radiofrequency fields," *Nano Research*, vol. 2, pp. 400-405, 2009.

[6] J. Cardinal, J. R. Klune, E. Chory, G. Jeyabalan, J. S. Kanzius, M. Nalesnik, and D. A. Geller, "Noninvasive radiofrequency ablation of cancer targeted by gold nanoparticles," *Surgery*, vol. 144, pp. 125-132, 2008.

[7] C. J. Gannon, P. Cherukuri, B. I. Yakobson, L. Cognet, J. S. Kanzius, C. Kittrell, R. B. Weisman, M. Pasquali, H. K. Schmidt, and R. E. Smalley, "Carbon nanotube-enhanced thermal destruction of cancer cells in a noninvasive radiofrequency field," *Cancer*, vol. 110, pp. 2654-2665, 2007.

[8] U. Gneveckow, A. Jordan, R. Scholz, V. Brüß, N. Waldöfner, J. Ricke, A. Feussner, B. Hildebrandt, B. Rau, and P. Wust, "Description and characterization of the novel hyperthermia-and thermoablation-system MFH300F for clinical magnetic fluid hyperthermia," *Medical Physics*, vol. 31, pp. 1444, 2004.

[9] A. Jordan, P. Wust, H. Fähling, W. John, A. Hinz, and R. Felix, "Inductive heating of ferrimagnetic particles and magnetic fluids: physical evaluation of their potential for hyperthermia," *International Journal Of Hyperthermia*, vol. 9, pp. 51-68, 1993.

[10] A. Jordan, R. Scholz, P. Wust, H. FaKhling, and R. Felix, "Magnetic fluid hyperthermia (MFH): Cancer treatment with AC magnetic" eld induced excitation of biocompatible superparamagnetic nanoparticles," *Journal of Magnetism and Magnetic Materials*, vol. 201, pp. 413-419, 1999.

[11] A. Jordan, R. Scholz, K. Maier-Hauff, M. Johannsen, P. Wust, J. Nadobny, H. Schirra, H. Schmidt, S. Deger, and S. Loening, "Presentation of a new magnetic field therapy system for the treatment of human solid tumors with magnetic fluid hyperthermia," *Journal of Magnetism and Magnetic Materials*, vol. 225, pp. 118-126, 2001.

[12] A. Jordan, R. Scholz, K. Maier-Hauff, F. K. H. van Landeghem, N. Waldoefner, U. Teichgraeber, J. Pinkernelle, H. Bruhn, F. Neumann, and B. Thiesen, "The effect of thermotherapy using magnetic nanoparticles on rat malignant glioma," *Journal of Neuro-Oncology*, vol. 78, pp. 7-14, 2006.

[13] M. Johannsen, A. Jordan, R. Scholz, M. Koch, M. Lein, S. Deger, J. Roigas, K. Jung, and S. Loening, "Evaluation of magnetic fluid hyperthermia in a standard rat model of prostate cancer," *Journal of Endourology*, vol. 18, pp. 495-500, 2004.

[14] K. Maier-Hauff, R. Rothe, R. Scholz, U. Gneveckow, P. Wust, B. Thiesen, A. Feussner, A. von Deimling, N. Waldoefner, R. Felix, and A. Jordan, "Intracranial thermotherapy using magnetic nanoparticles combined with external beam radiotherapy: results of a feasibility study on patients with glioblastoma multiforme," *Journal of Neuro-Oncology*, vol. 81, pp. 53-60, 2007.

[15] A. Jordan, T. Rheinländer, N. Waldöfner, and R. Scholz, "Increase of the specific absorption rate (SAR) by magnetic fractionation of magnetic fluids," *Journal of Nanoparticle Research*, vol. 5, pp. 597-600, 2003.

[16] J. Kanzius, "System and method for RF-induced hyperthermia (US20050251233A1, Pending)," US Patent Office, 2004.

[17] J. Kanzius, W. H. Steinbrink, R. J. McDonald, and M. J. Keating, "Systems and methods for RF-induced hyperthermia using biological cells and nanoparticles as RF enhancer carriers (US20050251234A1, Pending)," US Patent Office, 2005.

[18] J. Kanzius, W. H. Steinbrink, R. J. McDonald, and M. J. Keating, "Systems and methods for combined RF-induced hyperthermia and radioimmunotherapy (US20050273143A1, Pending)," US Patent Office, 2005.

[19] J. Kanzius, "Enhanced systems and methods for RF-induced hyperthermia (US20060190063A1, Pending)," US Patent Office, 2005.

[20] J. Kanzius, "Enhanced systems and methods for RF-induced hyperthermia II (US20070250139A1, Pending)," US Patent Office, 2005.

[21] A. S. Wright, F. T. Lee, and D. M. Mahvi, "Hepatic microwave ablation with multiple antennae results in synergistically larger zones of coagulation necrosis," vol. 10: Soc Surgical Oncol, 2003, pp. 275-283.

[22] J. C. Chen, J. A. Moriarty, J. A. Derbyshire, R. D. Peters, J. Trachtenberg, S. D. Bell, J. Doyle, R. Arrelano, G. A. Wright, and R. M. Henkelman, "Prostate Cancer: MR Imaging and Thermometry during Microwave Thermal Ablation-Initial Experience 1," vol. 214: RSNA, 2000, pp. 290-297.

[23] C. M. Hassan and N. A. Peppas, "Structure and applications of poly (vinyl alcohol) hydrogels produced by conventional crosslinking or by freezing/thawing methods," *Advances in Polymer Science*, vol. 153, pp. 37-66, 2000.

[24] J. L. Lyon, D. A. Fleming, M. B. Stone, P. Schiffer, and M. E. Williams, "Synthesis of Fe oxide core/Au shell nanoparticles by iterative hydroxylamine seeding," *Nano Lett*, vol. 4, pp. 719-723, 2004.

[25] K. Homan, J. Shah, S. Gomez, H. Gensler, A. Karpiouk, L. Brannon-Peppas, and S. Emelianov, "Combined ultrasound and photoacoustic imaging of pancreatic cancer using nanocage contrast agents," presented at SPIE Photonics West, 2009.

[26] R. E. Woodrough, *Medical infra-red thermography: principles and practice*, vol. 7. Cambridge, UK: Cambridge University Press, 1982.

Chapter 4: Conclusions

4.1 Motivation

RF/microwave hyperthermia guided by targeted nanoabsorbers is an efficient alternative to traditional cancer treatments. Electromagnetic energy, usually between 100 kHz and 10 GHz, is transmitted to the body where nanoparticles (NPs) transform the radiated energy into heat [1-11]. Selectively targeted NPs increase the energy absorption of the selected regions when exposed to microwave energy. Therefore, efficient heating can be achieved in a localized region making RF/microwave hyperthermia with targeted nanoabsorbers region specific as well as noninvasive.

Ultrasound imaging has been used to identify cancerous tissue anatomy and physiology [12,13]. In addition, ultrasound imaging can be used for treatment monitoring of temperature by tracking the thermally-induced motion of speckle in successive frames [14-17]. This temperature monitoring modality is relative inexpensive, noninvasive, and can acquire temperatures of deep tissue structures.

At microwave frequencies, the electromagnetic radiation does not interfere with ultrasound imaging. The combination of targeted microwave nanoabsorbers, microwave emission, and ultrasound temperature monitoring can provide an effective hyperthermia treatment. Therefore, the overall goal of this thesis is to demonstrate the ability of nanoparticles to transform microwave energy into heat for hyperthermia treatments, which may be utilized in the ablation of cancer.

4.2 Summary

Initially, correlations between differential temperatures and normalized time shifts for gelatin and porcine tissues were found (Chapter 2). Studies were performed on aqueous 8% porcine gelatin by weight, porcine *longissimus dorsi* muscle, and porcine fat. The test samples were heated between 15˚C and 25˚C in a water bath to assure even temperature distribution within the samples. Ultrasound images were acquired every 0.5˚C and the apparent time shifts in the RF signals were measured. Spatial gradients were calculated from the apparent time shifts and correlated with differential temperature.

Determination of microwave energy nanoabsorbers were conducted (Chapter 3) using infrared emissions as the measure of absorption. Six different nanoparticles were selected and subjected to a 10 minute exposure of 2.45 GHz microwave irradiation. Maghemite proved to be the best converter of microwave energy to heat, due to its size and electrical conductivity. An *ex-vivo* experiment with porcine *longissimus dorsi* muscle tissue was carried out with 20 nm magnetite. Temperature was monitored using ultrasound speckle motion tracking during a one minute microwave treatment. Results show that large differential temperatures were induced in the region with inoculations of magnetite nanoparticles.

4.3 Limitations

4.3.1 Ultrasound Temperature Monitoring

Due to the nature of tracking the ultrasound speckle, motion within the ultrasound frame not induced by the temperature dependency of the speed of sound may cause artifacts in temperature. In the clinical setting, tissue motion will occur due to respiration and cardiac cycles. Since thermal time shifts are on the order of 0.1 mm for 5˚C changes in temperature, respiration and cardiac cycle motion will cause incorrect readings. MR thermal imaging also has motion artifact from patient motion [18,19]. Temperature motion artifacts in ultrasound temperature monitoring can be reduced by triggering the ultrasound image acquisition based on physiological signals.

4.3.2 Microwave Hyperthermia using Microwave Nanoabsorbers

Electromagnetic energy propagating through tissue in the microwave band has high energy attenuation, as shown in Figure 1.1. This fundamental problem has plagued microwave hyperthermia scientists. Since many cancers lie deep within the body, microwave hyperthermia is usually an invasive technique. Attenuation of electromagnetic energy can be reduced within the body by lowering the frequency. Coupling to nanoparticles that absorb energy at lower frequencies can combat deep lying cancers.

4.4 Future Directions

RF energy at 100 kHz, 150 kHz, and 13.56 kHz in conjunction with nanoparticles has been shown to effectively increase differential temperatures in tissues

[1-11]. Most investigators utilize a pair of transceivers placed on opposing sides of the targeted tissue region. This places tissues between the transceivers in series. Therefore, much of the energy can be absorbed in surface structures, such as fat. RF applicators, such as inductive coil, place the tissue structures in parallel and can allow for more heating in the nanoparticle targeted region because of a reduction in conductivity. Pancake coils can project the electromagnetic field at low radio frequencies; thus, allowing for more localized treatments.

Although nanoparticles have been shown to be effective with RF and microwave absorption, absorption spectra for particle types and sizes have not been characterized. The electromagnetic absorption spectra for nanoparticles define the therapeutic efficiency for this modality. In addition, knowledge of the size dependence on frequency for particular nanoparticle types can prove useful in a nanoparticle design for therapy.

Another area that can be explored utilizes the thermoacoustic response from pulsed RF/microwave energy. This response is acquired with an ultrasound transducer and then translated into a spatially resolved image. Microwave thermoacoustic imaging, much like photoacoustic imaging, is an acoustic pulse amplitude imaging modality [18-21]. For deep lying structures, combining continuous wave RF with pulsed RF emissions can therapeutically treat cancers and monitor temperature. Since thermoacoustic imaging relies on amplitude, instead of speckle location, motion artifacts do not affect the image when the image is combined with normal ultrasound

imaging. Thermoacoustic imaging can also detect RF absorbing nanoparticles; thus, can aid in pre-therapy treatment planning.

4.5 Concluding Remarks

A combined microwave emitter, microwave absorbing nanoparticles, and ultrasound temperature monitoring system was described to effectively induce therapeutic hyperthermia. In this study, effective microwave nanoabsorbers were determined from several nanoparticle types by monitoring their energy conversion to heat with an infrared thermal camera. The microwave nanoabsorber was then tested in an *ex-vivo longissimus dorsi* porcine muscle sample. Thermal images from ultrasound speckle tracking revealed differential temperatures between nanoabsorber inclusions and surrounding medium.

Further studies of RF/microwave nanoabsorber absorption spectra are needed. Applicator designs that involve projecting the electromagnetic field into the body to minimize equipment size and patient discomfort should be explored. In addition, thermoacoustic or photoacoustic ultrasound imaging needs to be explored to better guide and monitor therapy. Overall, electromagnetic nanoabsorbers have proven to effectively focus heat within a targeted region during non-invasive microwave irradiation.

4.6 References

[1] C. H. Moran, S. M. Wainerdi, T. K. Cherukuri, C. Kittrell, B. J. Wiley, N. W. Nicholas, S. A. Curley, J. S. Kanzius, and P. Cherukuri, "Size-dependent joule heating of gold nanoparticles using capacitively coupled radiofrequency fields," *Nano Research*, vol. 2, pp. 400-405, 2009.

[2] J. Cardinal, J. R. Klune, E. Chory, G. Jeyabalan, J. S. Kanzius, M. Nalesnik, and D. A. Geller, "Noninvasive radiofrequency ablation of cancer targeted by gold nanoparticles," *Surgery*, vol. 144, pp. 125-132, 2008.

[3] C. J. Gannon, P. Cherukuri, B. I. Yakobson, L. Cognet, J. S. Kanzius, C. Kittrell, R. B. Weisman, M. Pasquali, H. K. Schmidt, and R. E. Smalley, "Carbon nanotube-enhanced thermal destruction of cancer cells in a noninvasive radiofrequency field," *Cancer*, vol. 110, pp. 2654-2665, 2007.

[4] U. Gneveckow, A. Jordan, R. Scholz, V. Brüß, N. Waldöfner, J. Ricke, A. Feussner, B. Hildebrandt, B. Rau, and P. Wust, "Description and characterization of the novel hyperthermia-and thermoablation-system MFH300F for clinical magnetic fluid hyperthermia," *Medical Physics*, vol. 31, pp. 1444, 2004.

[5] A. Jordan, P. Wust, H. Fähling, W. John, A. Hinz, and R. Felix, "Inductive heating of ferrimagnetic particles and magnetic fluids: physical evaluation of their potential for hyperthermia," *International Journal Of Hyperthermia*, vol. 9, pp. 51-68, 1993.

[6] A. Jordan, R. Scholz, P. Wust, H. FaKhling, and R. Felix, "Magnetic fluid hyperthermia (MFH): Cancer treatment with AC magnetic" eld induced excitation of biocompatible superparamagnetic nanoparticles," *Journal of Magnetism and Magnetic Materials*, vol. 201, pp. 413-419, 1999.

[7] A. Jordan, R. Scholz, K. Maier-Hauff, M. Johannsen, P. Wust, J. Nadobny, H. Schirra, H. Schmidt, S. Deger, and S. Loening, "Presentation of a new magnetic field therapy system for the treatment of human solid tumors with magnetic fluid hyperthermia," *Journal of Magnetism and Magnetic Materials*, vol. 225, pp. 118-126, 2001.

[8] A. Jordan, R. Scholz, K. Maier-Hauff, F. K. H. van Landeghem, N. Waldoefner, U. Teichgraeber, J. Pinkernelle, H. Bruhn, F. Neumann, and B. Thiesen, "The effect of thermotherapy using magnetic nanoparticles on rat malignant glioma," *Journal of Neuro-Oncology*, vol. 78, pp. 7-14, 2006.

[9] M. Johannsen, A. Jordan, R. Scholz, M. Koch, M. Lein, S. Deger, J. Roigas, K. Jung, and S. Loening, "Evaluation of magnetic fluid hyperthermia in a standard rat model of prostate cancer," *Journal of Endourology*, vol. 18, pp. 495-500, 2004.

[10] K. Maier-Hauff, R. Rothe, R. Scholz, U. Gneveckow, P. Wust, B. Thiesen, A. Feussner, A. von Deimling, N. Waldoefner, R. Felix, and A. Jordan, "Intracranial thermotherapy using magnetic nanoparticles combined with external beam radiotherapy: results of a feasibility study on patients with glioblastoma multiforme," *Journal of Neuro-Oncology*, vol. 81, pp. 53-60, 2007.

[11] A. Jordan, T. Rheinländer, N. Waldöfner, and R. Scholz, "Increase of the specific absorption rate (SAR) by magnetic fractionation of magnetic fluids," *Journal of Nanoparticle Research*, vol. 5, pp. 597-600, 2003.

[12] B. Y. Karlan and L. D. Platt, "Ovarian cancer screening. The role of ultrasound in early detection," *Cancer*, vol. 76, pp. 2011-2015, 1995.

[13] W. Teh and A. R. M. Wilson, "The role of ultrasound in breast cancer screening. A consensus statement by the European Group for Breast Cancer Screening," *European Journal of Cancer*, vol. 34, pp. 449-450, 1998.

[14] R. Seip, P. VanBaren, C. Simon, and E. S. Ebbini, "Non-invasive spatio-temporal temperature estimation using diagnostic ultrasound," presented at IEEE Ultrasonics Symposium, 1995.

[15] J. Shah, S. R. Aglyamov, K. Sokolov, T. E. Milner, and S. Y. Emelianov, "Ultrasound-based thermal and elasticity imaging to assist photothermal cancer therapy-Preliminary study," presented at IEEE Ultrasonics Symposium, 2006.

[16] J. Shah, S. R. Aglyamov, K. Sokolov, T. E. Milner, and S. Y. Emelianov, "Ultrasound imaging to monitor photothermal therapy–Feasibility study," *Optics Express*, vol. 16, pp. 3776-3785, 2008.

[17] T. Varghese, J. A. Zagzebski, Q. Chen, U. Techavipoo, G. Frank, C. Johnson, A. Wright, and F. T. Lee Jr, "Ultrasound monitoring of temperature change during radiofrequency ablation: preliminary in-vivo results," *Ultrasound in Medicine & Biology*, vol. 28, pp. 321-329, 2002.

[18] G. Ku and L. V. Wang, "Scanning thermoacoustic tomography in biological tissue," *Medical Physics*, vol. 27, pp. 1195-1202, 2000.

[19] G. Ku and L. V. Wang, "Scanning microwave-induced thermoacoustic tomography: signal, resolution, and contrast," *Medical Physics*, vol. 28, pp. 4-10, 2001.

[20] Y. Xu, M. Xu, and L. V. Wang, "Exact frequency-domain reconstruction for thermoacoustic tomography—II: cylindrical geometry," *IEEE Transactions on Medical Imaging*, vol. 21, pp. 829-833, 2002.

[21] R. A. Kruger, D. R. Reinecke, and G. A. Kruger, "Thermoacoustic computed tomography–technical considerations," *Medical Physics*, vol. 26, pp. 1832-1837, 1999.

Bibliography

"Cancer facts and figures 2009," American Cancer Society.

M. R. Bailey, V. A. Khokhlova, O. A. Sapozhnikov, S. G. Kargl, and L. A. Crum, "Physical mechanisms of the therapeutic effect of ultrasound (a review)," *Acoustical Physics*, vol. 49, pp. 369-388, 2003.

J. T. Beckham, M. A. Mackanos, C. Crooke, T. Takahashi, C. O'Connell-Rodwell, C. H. Contag, and E. Duco Jansen, "Assessment of cellular response to thermal laser injury through bioluminescence imaging of heat shock protein 70," *Photochemistry and Photobiology*, vol. 79, pp. 76-85, 2004.

R. Birngruber, *Thermal modeling in biological tissue*. New York: Plenum Press, 1980.

R. Birngruber, F. Hillenkamp, and V. P. Gabel, "Theoretical investigations of laser thermal retinal injury," *Health Physics*, vol. 48, pp. 781-796, 1985.

R. Brinkmann, B. Radt, C. Flamm, J. Kampmeier, N. Koop, and R. Birngruber, "Influence of temperature and time on thermally induced forces in corneal collagen and the effect on laser thermokeratoplasty," *Journal of Cataract & Refractive Surgery*, vol. 26, pp. 744-754, 2000.

P. C. Brown, R. Consden, and L. E. Glynn, "Observations on the Shrink Temperature of Collagen and its Variations with Age and Disease," *British Medical Journal*, vol. 17, pp. 196, 1958.

J. Cardinal, J. R. Klune, E. Chory, G. Jeyabalan, J. S. Kanzius, M. Nalesnik, and D. A. Geller, "Noninvasive radiofrequency ablation of cancer targeted by gold nanoparticles," *Surgery*, vol. 144, pp. 125-132, 2008.

Y. A. Cengel and M. A. Boles, *Thermodynamics: an engineering approach*, 4 ed. New York: McGraw Hill, 2002.

D. C. F. Chan, D. B. Kirpotin, and P. A. Bunn, "Synthesis and evaluation of colloidal magnetic iron oxides for the site-specific radiofrequency-induced hyperthermia of cancer," *Journal of Magnetism and Magnetic Materials*, vol. 122, pp. 374-378, 1993.

J. C. Chen, J. A. Moriarty, J. A. Derbyshire, R. D. Peters, J. Trachtenberg, S. D. Bell, J. Doyle, R. Arrelano, G. A. Wright, and R. M. Henkelman, "Prostate Cancer: MR Imaging and Thermometry during Microwave Thermal Ablation-Initial Experience 1," vol. 214: RSNA, 2000, pp. 290-297.

S. Chikazumi, *Physics of Magnetism*. Philadelphia, PA: Lippincott, 1964.

K. S. Cole and R. H. Cole, "Dispersion and absorption in dielectrics I. Alternating current characteristics," *The Journal of Chemical Physics*, vol. 9, pp. 341, 1941.
C. R. Company, *CRC handbook of chemistry and physics*, 69 ed. Boca Raton, Florida: CRC Press, Inc., 1988.

B. Decadt and A. K. Siriwardena, "Radiofrequency ablation of liver tumours: systematic review," *Lancet Oncology*, vol. 5, pp. 550-560, 2004.

K. R. Diller, J. A. Pearce, and J. W. Valvano, "Bioheat transfer," in *The CRC Handbook of Mechanical Engineering*, F. Kreith and D. Y. Goswami, Eds.: CRC Press, 2000, pp. 4.114-4.187.

M. Dollinger, E. H. Rosenbaum, M. Tempero, and S. J. Mulvihill, *Everyone's guide to cancer therapy: how cancer is diagnosed, treated, and managed day to day*, 4 ed: Andrews McMeel Publishing, 2002.

O. C. Farokhzad, S. Jon, A. Khademhosseini, T. N. T. Tran, D. A. LaVan, and R. Langer, "Nanoparticle-Aptamer Bioconjugates A New Approach for Targeting Prostate Cancer Cells," vol. 64: AACR, 2004, pp. 7668-7672.

O. C. Farokhzad, J. M. Karp, and R. Langer, "Nanoparticle-aptamer bioconjugates for cancer targeting," *Expert Opin. Drug Deliv.*, vol. 3, pp. 311-324, 2006.

S. T. Flock, L. Smith, and M. Waner, "Quantifying the effects on blood of irradiation with four different vascular-lesion lasers," presented at SPIE: Laser-Tissue Interaction IV, 1993.

C. E. Fugitt, "A rate process of thermal injury," *Armed Forces Special Weapons Project AFSWP-606*, 1955.

C. J. Gannon, P. Cherukuri, B. I. Yakobson, L. Cognet, J. S. Kanzius, C. Kittrell, R. B. Weisman, M. Pasquali, H. K. Schmidt, and R. E. Smalley, "Carbon nanotube-enhanced thermal destruction of cancer cells in a noninvasive radiofrequency field," *Cancer*, vol. 110, pp. 2654-2665, 2007.

X. Gao, Y. Cui, R. M. Levenson, L. W. K. Chung, and S. Nie, "In vivo cancer targeting and imaging with semiconductor quantum dots," *Nature Biotechnology*, vol. 22, pp. 969-976, 2004.

D. C. Gaylor, *Physical mechanisms of cellular injury in electrical trauma*: Massachuszetts Institute of Technology, 1989.

I. M. Germano, Y. F. Zhang, E. F. Sperber, and S. L. Moshe, "Neuronal migration disorders increase susceptibility to hyperthermia-induced seizures in developing rats," *Epilepsia*, vol. 37, pp. 902-910, 1996.

R. K. Gilchrist, R. Medal, W. D. Shorey, R. C. Hanselman, J. C. Parrott, and C. B. Taylor, "Selective inductive heating of lymph nodes," *Annals of Surgery*, vol. 146, pp. 596-606, 1957.

U. Gneveckow, A. Jordan, R. Scholz, V. Brüß, N. Waldöfner, J. Ricke, A. Feussner, B. Hildebrandt, B. Rau, and P. Wust, "Description and characterization of the novel hyperthermia-and thermoablation-system MFH300F for clinical magnetic fluid hyperthermia," *Medical Physics*, vol. 31, pp. 1444, 2004.

C. L. Holloway, R. R. DeLyser, R. F. German, P. McKenna, and M. Kanda, "Comparison of electromagnetic absorber used in anechoic andsemi-anechoic chambers for emissions and immunity testing of digitaldevices," *IEEE Transactions on Electromagnetic Compatibility*, vol. 39, pp. 33-47, 1997.

A. H. Habib, C. L. Ondeck, P. Chaudhary, M. R. Bockstaller, and M. E. McHenry, "Evaluation of iron-cobalt/ferrite core-shell nanoparticles for cancer thermotherapy," *Journal of Applied Physics*, vol. 103, pp. 07A307, 2008.

D. M. Hall, G. R. Buettner, L. W. Oberley, L. Xu, R. D. Matthes, and C. V. Gisolfi, "Mechanisms of circulatory and intestinal barrier dysfunction during whole body hyperthermia," *American Journal of Physiology - Heart and Circulatory Physiology*, vol. 280, pp. 509-521, 2001.

R. Hamazoe, M. Maeta, A. Murakami, H. Yamashiro, and N. Kaibara, "Heating efficiency of radiofrequency capacitive hyperthermia for treatment of deep-seated tumors in the peritoneal cavity," *Journal of Surgical Oncology*, vol. 48, pp. 176-179, 1991.

C. M. Hassan and N. A. Peppas, "Structure and applications of poly (vinyl alcohol) hydrogels produced by conventional crosslinking or by freezing/thawing methods," *Advances in Polymer Science*, vol. 153, pp. 37-66, 2000.

X. He, S. McGee, J. E. Coad, F. Schmidlin, P. A. Iaizzo, D. J. Swanlund, S. Kluge, E. Rudie, and J. C. Bischof, "Investigation of the thermal and tissue injury behaviour in microwave thermal therapy using a porcine kidney model," *International Journal of Hyperthermia*, vol. 20, pp. 567-593, 2004.

F. C. Henriques and A. R. Moritz, "Studies of thermal injury: I. the conduction of heat to and through skin and the temperatures attained therein," *Am. J. Pathol*, vol. 23, pp. 531-549, 1947.

R. Hergt, W. Andra, C. G. d'Ambly, I. Hilger, W. A. Kaiser, U. Richter, and H. G. Schmidt, "Physical limits of hyperthermia using magnetite fine particles," *IEEE Transactions on Magnetics*, vol. 34, pp. 3745-3754, 1998.

R. Hergt, W. Andra, C. G. d'Ambly, I. Hilger, W. A. Kaiser, U. Richter, and H. G. Schmidt, "Physical limits of hyperthermia using magnetite fine particles," *IEEE Transactions on Magnetics*, vol. 34, pp. 3745-3754, 1998.

L. R. Hirsch, R. J. Stafford, J. A. Bankson, S. R. Sershen, B. Rivera, R. E. Price, J. D. Hazle, N. J. Halas, and J. L. West, "Nanoshell-mediated near-infrared thermal therapy of tumors under magnetic resonance guidance," *Proceedings of the National Academy of Sciences*, vol. 100, pp. 13549-13554, 2003.

K. Homan, J. Shah, S. Gomez, H. Gensler, A. Karpiouk, L. Brannon-Peppas, and S. Emelianov, "Combined ultrasound and photoacoustic imaging of pancreatic cancer using nanocage contrast agents," presented at SPIE Photonics West, 2009.

X. Huang, P. K. Jain, I. H. El-Sayed, and M. A. El-Sayed, "Plasmonic photothermal therapy (PPTT) using gold nanoparticles," *Lasers in Medical Science*, vol. 23, pp. 217-228, 2008.

X. Huang, I. H. El-Sayed, W. Qian, and M. A. El-Sayed, "Cancer cell imaging and photothermal therapy in the near-infrared region by using gold nanorods," *J. Am. Chem. Soc*, vol. 128, pp. 2115-2120, 2006.

F. P. Incropera and D. P. DeWitt, *Fundamental of heat and mass transfer*, 4 ed. New York: John Wiley & Sons, 1996.

S. L. Jacques and M. O. Gaeeni, "Thermally induced changes in optical properties of heart," presented at IEEE Engineering in Medicine and Biology, 1989.

S. L. Jacques, M. Motamedi, and S. Rastegar, "Computer simulation of laser coagulation of prostate: a guide to dosimetry. American Society for Lasers in Medicine and Surgery," *Lasers Surg. Med. Suppl*, vol. 5, pp. abstract 311, 1993.

S. L. Jacques and C. Newman, "Thermal coagulation of tissues: liver studies indicate a distribution of rate parameters, not a single rate parameter, describes the coagulation process," presented at Annual Winter Meeting of the American Society of Mechanical Engineers, 1991.

S. L. Jacques and S. A. Prahl, "Modeling optical and thermal distributions in tissue during laser irradiation," *Lasers in Surgery and Medicine*, vol. 6, pp. 494-503, 1987.

C. C. Johnson and A. W. Guy, "Nonionizing electromagnetic wave effects in biological materials and systems," *Proceedings of the IEEE*, vol. 60, pp. 692-718, 1972.

M. Johannsen, A. Jordan, R. Scholz, M. Koch, M. Lein, S. Deger, J. Roigas, K. Jung, and S. Loening, "Evaluation of magnetic fluid hyperthermia in a standard rat model of prostate cancer," *Journal of Endourology*, vol. 18, pp. 495-500, 2004.

A. Jordan, T. Rheinländer, N. Waldöfner, and R. Scholz, "Increase of the specific absorption rate (SAR) by magnetic fractionation of magnetic fluids," *Journal of Nanoparticle Research*, vol. 5, pp. 597-600, 2003.

A. Jordan, R. Scholz, P. Wust, H. FaKhling, and R. Felix, "Magnetic fluid hyperthermia (MFH): Cancer treatment with AC magnetic" eld induced excitation of biocompatible superparamagnetic nanoparticles," *Journal of Magnetism and Magnetic Materials*, vol. 201, pp. 413-419, 1999.

A. Jordan, R. Scholz, K. Maier-Hauff, M. Johannsen, P. Wust, J. Nadobny, H. Schirra, H. Schmidt, S. Deger, and S. Loening, "Presentation of a new magnetic field therapy system for the treatment of human solid tumors with magnetic fluid hyperthermia," *Journal of Magnetism and Magnetic Materials*, vol. 225, pp. 118-126, 2001.

A. Jordan, R. Scholz, K. Maier-Hauff, F. K. H. van Landeghem, N. Waldoefner, U. Teichgraeber, J. Pinkernelle, H. Bruhn, F. Neumann, and B. Thiesen, "The effect of thermotherapy using magnetic nanoparticles on rat malignant glioma," *Journal of Neuro-Oncology*, vol. 78, pp. 7-14, 2006.

A. Jordan, P. Wust, H. Fähling, W. John, A. Hinz, and R. Felix, "Inductive heating of ferrimagnetic particles and magnetic fluids: physical evaluation of their potential for hyperthermia," *International Journal Of Hyperthermia*, vol. 9, pp. 51-68, 1993.

J. Kanzius, "System and method for RF-induced hyperthermia (US20050251233A1, Pending)," US Patent Office, 2004.

J. Kanzius, W. H. Steinbrink, R. J. McDonald, and M. J. Keating, "Systems and methods for RF-induced hyperthermia using biological cells and nanoparticles as RF enhancer carriers (US20050251234A1, Pending)," US Patent Office, 2005.

J. Kanzius, W. H. Steinbrink, R. J. McDonald, and M. J. Keating, "Systems and methods for combined RF-induced hyperthermia and radioimmunotherapy (US20050273143A1, Pending)," US Patent Office, 2005.

J. Kanzius, "Enhanced systems and methods for RF-induced hyperthermia (US20060190063A1, Pending)," US Patent Office, 2005.

J. Kanzius, "Enhanced systems and methods for RF-induced hyperthermia II (US20070250139A1, Pending)," US Patent Office, 2005.

B. Y. Karlan and L. D. Platt, "Ovarian cancer screening. The role of ultrasound in early detection," *Cancer*, vol. 76, pp. 2011-2015, 1995.

B. Khlebtsov, V. Zharov, A. Melnikov, V. Tuchin, and N. Khlebtsov, "Optical amplification of photothermal therapy with gold nanoparticles and nanoclusters," *Nanotechnology*, vol. 17, pp. 5167-5179, 2006.

E. Kneller, *Theory of the magnetization curve of small crystals*, vol. 18, 2 ed. New York: Springer-Verlag, 1966.

R. A. Kruger, D. R. Reinecke, and G. A. Kruger, "Thermoacoustic computed tomography–technical considerations," *Medical Physics*, vol. 26, pp. 1832-1837, 1999.

G. Ku and L. V. Wang, "Scanning thermoacoustic tomography in biological tissue," *Medical Physics*, vol. 27, pp. 1195-1202, 2000.

G. Ku and L. V. Wang, "Scanning microwave-induced thermoacoustic tomography: signal, resolution, and contrast," *Medical Physics*, vol. 28, pp. 4-10, 2001.

J. R. Lepock, H. E. Frey, H. Bayne, and J. Markus, "Relationship of hyperthermia-induced hemolysis of human erythrocytes to the thermal denaturation of membrane proteins," *Biochimica et Biophysica Acta*, vol. 980, pp. 191-201, 1989.

T. Livraghi, S. N. Goldberg, S. Lazzaroni, F. Meloni, T. Ierace, L. Solbiati, and G. S. Gazelle, "Hepatocellular carcinoma: radio-frequency ablation of medium and large lesions," *Radiology*, vol. 214, pp. 761-768, 2000.

C. Loo, A. Lowery, N. Halas, J. West, and R. Drezek, "Immunotargeted nanoshells for integrated cancer imaging and therapy," *Nano Letters*, vol. 5, pp. 709-712, 2005.

J. L. Lyon, D. A. Fleming, M. B. Stone, P. Schiffer, and M. E. Williams, "Synthesis of Fe oxide core/Au shell nanoparticles by iterative hydroxylamine seeding," *Nano Letters*, vol. 4, pp. 719-723, 2004.

R. Maas-Moreno and C. Damianou, "Noninvasive temperature estimation in tissue via ultrasound echoshifts, parts 1 and 2," *Journal of the Acoustal Society of America*, vol. 100, pp. 2514-2530, 1996.

K. Maier-Hauff, R. Rothe, R. Scholz, U. Gneveckow, P. Wust, B. Thiesen, A. Feussner, A. von Deimling, N. Waldoefner, R. Felix, and A. Jordan, "Intracranial thermotherapy using magnetic nanoparticles combined with external beam radiotherapy: results of a feasibility study on patients with glioblastoma multiforme," *Journal of Neuro-Oncology*, vol. 81, pp. 53-60, 2007.

D. J. Maitland and J. T. Walsh Jr, "Quantitative measurements of linear birefringence during heating of native collagen," *Lasers in Surgery and Medicine*, vol. 20, pp. 310-318, 1997.

K. Matthewson, P. Coleridge-Smith, J. P. O'Sullivan, T. C. Northfield, and S. G. Brown, "Biological effects of intrahepatic neodymium: yttrium-aluminum-garnet laser photocoagulation in rats," *Gastroenterology (New York, NY. 1943)*, vol. 93, pp. 550-557, 1987.

C. A. Miles, "Kinetics of collagen denaturation in mammalian lens capsules studied by differential scanning calorimetry," *International Journal of Biological Macromolecules*, vol. 15, pp. 265, 1993.

N. R. Miller, J. C. Bamber, and G. R. ter Haar, "Imaging of temperature-induced echo strain: preliminary in vitro study to assess feasibility for guiding focused ultrasound surgery," *Ultrasound in Medicine & Biology*, vol. 30, pp. 345-356, 2004.

S. Mizushina, *Non-invasive temperature measurement*: Gordan and Breach Science Publishers, 1988.

C. H. Moran, S. M. Wainerdi, T. K. Cherukuri, C. Kittrell, B. J. Wiley, N. W. Nicholas, S. A. Curley, J. S. Kanzius, and P. Cherukuri, "Size-dependent joule heating of gold nanoparticles using capacitively coupled radiofrequency fields," *Nano Research*, vol. 2, pp. 400-405, 2009.

A. R. Moritz, "Studies of thermal injury: III. the pathology and pathogenesis of cutaneous burns. an experimental study*," *The American Journal of Pathology*, vol. 23, pp. 915-934, 1947.

A. R. Moritz and F. C. Henriquez, "Studies of thermal iInjury: II. the relative importance of time and surface temperature in the causation of cutaneous burns," *The American Journal of Pathology*, vol. 23, pp. 693-720, 1947.

S. Mornet, S. Vasseur, F. Grasset, and E. Duguet, "Magnetic nanoparticle design for medical diagnosis and therapy," *Journal of Materials Chemistry*, vol. 14, pp. 2161-2175, 2004.

N. A. Moussa, E. N. Tell, and E. G. Cravalho, "Time progression of hemolysis of erythrocyte populations exposed to supraphysiological temperatures," *Journal of Biomechanical Engineering*, vol. 101, pp. 213-217, 1979.

R. L. Nasoni, "Temperature corrected speed of sound for use in soft tissue imaging," *Medical Physics*, vol. 8, pp. 513-515, 1981.

J. A. Pearce, "Relationship between Arrhenius models of thermal damage and the CEM 43 thermal dose," presented at SPIE, 2009.

J. A. Pearce and S. L. Thomsen, "Thermal damage parameters from laser coagulation experiments," presented at SPIE, 2003.

J. A. Pearce, S. L. Thomsen, H. Vijverberg, and T. J. McMurray, "Kinetics for birefringence changes in thermally coagulated rat skin collagen," presented at SPIE, 1993.

H. H. Pennes, "Analysis of tissue and arterial blood temperatures in the resting human forearm," *Journal of Applied Physiology*, vol. 1, pp. 93-122, 1948.

M. Pop, A. Molckovsky, L. Chin, M. C. Kolios, M. A. S. Jewett, and M. D. Sherar, "Changes in dielectric properties at 460 kHz of kidney and fat during heating: importance for radio-frequency thermal therapy," *Physics in Medicine and Biology*, vol. 48, pp. 2509-2526, 2003.

N. P. Praetorius and T. K. Mandal, "Engineered nanoparticles in cancer therapy," *Recent Patents on Drug Delivery and Formulation*, vol. 1, pp. 37-51, 2007.

B. Rajagopalan, J. F. Greenleaf, P. J. Thomas, S. A. Johnson, and R. C. Bahn, "Variation of acoustic speed with temperature in various excised human tissues studied by ultrasound computerized tomography," *Ultrasonic Tissue Characterization II. National Bureau of Standards, Washington DC*, pp. 227-233, 1979.

O. V. Salata, "Applications of nanoparticles in biology and medicine," *Journal of Nanobiotechnology*, vol. 2, pp. 3, 2004.

S. A. Sapareto, *Physical aspects of hyperthermia*: American Association of Physicists in Medicine, American Institute of Physics, 1982.

R. Seip, P. VanBaren, C. Simon, and E. S. Ebbini, "Non-invasive spatio-temporal temperature estimation using diagnostic ultrasound," presented at IEEE Ultrasonics Symposium, 1995.

J. Shah, "Ultrasound and photoacoustic imaging to guide and monitor photothermal therapy," Ph.D dissertation, University of Texas at Austin, Austin, TX, 2008.

J. Shah, S. R. Aglyamov, K. Sokolov, T. E. Milner, and S. Y. Emelianov, "Ultrasound-based thermal and elasticity imaging to assist photothermal cancer therapy-Preliminary study," presented at IEEE Ultrasonics Symposium, pp. 1029-1032, 2006.

J. Shah, S. R. Aglyamov, K. Sokolov, T. E. Milner, and S. Y. Emelianov, "Ultrasound imaging to monitor photothermal therapy–Feasibility study," *Optics Express*, vol. 16, pp. 3776-3785, 2008.

J. Shah, S. Park, S. Aglyamov, T. Larson, L. Ma, K. Sokolov, K. Johnston, T. Milner, and S. Emelianov, "Photoacoustic and ultrasound imaging to guide photothermal therapy: ex vivo study," presented at SPIE, vol. 6856m oo, 68560U:1-7, 2008.

J. Shah, S. Thomsen, T. E. Milner, and S. Y. Emelianov, "Ultrasound guidance and monitoring of laser-based fat removal," *Lasers in Surgery and Medicine*, vol. 40, pp. 680-687, 2008.

J. Y. Shin and J. H. Oh, "The microwave absorbing phenomena of ferrite microwave absorbers," *IEEE Transactions on Magnetics*, vol. 29, pp. 3437-3439, 1993.

M. G. Skinner, S. Everts, A. D. Reid, I. A. Vitkin, L. Lilge, and M. D. Sherar, "Changes in optical properties of ex vivo rat prostate due to heating," *Physics in Medicine and Biology*, vol. 45, pp. 1375-1386, 2000.

C. J. Simon, D. E. Dupuy, and W. W. Mayo-Smith, "Microwave ablation: principles and applications 1," *Radiographics*, vol. 25, pp. 69-83, 2005.

C. Simon, P. VanBaren, and E. Ebbini, "Quantitative analysis and applications of non-invasive temperature estimation using diagnostic ultrasound," presented at IEEE Ultrasounics Symposium, 1997.

W. L. Straube and R. M. Arthur, "Theoretical estimation of the temperature dependence of backscattered ultrasonic power for noninvasive thermometry," *Ultrasound in Medicine & Biology*, vol. 20, pp. 915-922, 1994.

A. N. Takata, "Development of criterion for skin burns," *Aerospace Med*, vol. 45, pp. 634-637, 1974.

A. N. Takata, L. Goldfinch, J. K. Hinds, L. P. Kuan, and N. Thomopoulis, "Thermal model of laser-induced eye damage," in *Acoustical Physics*: Storming Media, 1974.

W. Teh and A. R. M. Wilson, "The role of ultrasound in breast cancer screening. A consensus statement by the European Group for Breast Cancer Screening," *European Journal of Cancer*, vol. 34, pp. 449-450, 1998.

S. Ueno, M. Hashimoto, H. Fukukita, and T. Yano, "Ultrasound thermometry in hyperthermia," presented at IEEE Ultrasonics Symposium, 1990.

P. P. Vaishnava, R. Tackett, A. Dixit, C. Sudakar, R. Naik, and G. Lawes, "Magnetic relaxation and dissipative heating in ferrofluids," *Journal of Applied Physics*, vol. 102, pp. 063914, 2007.

C. T. Vangsness, W. Mitchell, M. Nimni, M. Erlich, V. Saadat, and H. Schmotzer, "Collagen shortening," *Clin Orthop*, vol. 337, pp. 267-71, 1997.

T. Varghese, J. A. Zagzebski, Q. Chen, U. Techavipoo, G. Frank, C. Johnson, A. Wright, and F. T. Lee Jr, "Ultrasound monitoring of temperature change during radiofrequency ablation: preliminary in-vivo results," *Ultrasound in Medicine & Biology*, vol. 28, pp. 321-329, 2002.

A. Vassiliadis, H. C. Zweng, K. G. Dedrick, and C. Stanford Research Institute Menlo Park, "Ocular laser threshold investigations," Stanford Research Institute Menlo Park California, 1971.

A. Vorst, A. Rosen, and Y. Kotsuka, *RF/microwave interaction with biological tissues*. New York: John Wiley & Sons, 2006.

J. A. Weaver and A. M. Stoll, "Mathematical model of skin exposed to thermal radiation," *Aerospace Medical*, vol. 40, pp. 24-30, 1969.

A. J. Welch and M. J. C. v. Gemert, *Optical-thermal response of laser-irradiated tissue*. New York: Springer, 1995.

A. J. Welch and G. D. Polhamus, "Measurement and prediction of thermal injury in the retina of the rhesus monkey," *IEEE Transactions on Biomedical Engineering*, vol. 31, pp. 633-644, 1984.

E. H. Wissler, "Pennes'1948 paper revisited," *Journal of Applied Physiology*, vol. 85, pp. 35-41, 1998.

R. E. Woodrough, *Medical infra-red thermography: principles and practice*, vol. 7. Cambridge, UK: Cambridge University Press, 1982.

A. S. Wright, F. T. Lee, and D. M. Mahvi, "Hepatic microwave ablation with multiple antennae results in synergistically larger zones of coagulation necrosis," *Radiographics*, vol. 10, pp. 275-283, 2003.

Y. C. Wu, "A modified criterion for predicting thermal injury," *National Bureau of Standards, Washington, District of Columbia*, 1982.

P. Wust, B. Hildebrandt, G. Sreenivasa, B. Rau, J. Gellermann, H. Riess, R. Felix, and P. M. Schlag, "Hyperthermia in combined treatment of cancer," *The Lancet Oncology*, vol. 3, pp. 487-497, 2002.

Y. Xu, M. Xu, and L. V. Wang, "Exact frequency-domain reconstruction for thermoacoustic tomography—II: cylindrical geometry," *IEEE Transactions on Medical Imaging*, vol. 21, pp. 829-833, 2002.

Y. Yang, A. J. Welch, and H. G. Rylander Iii, "Rate process parameters of albumen," *Lasers in Surgery and Medicine*, vol. 11, pp. 188-190, 1991.

A. N. Yusoff, M. H. Abdullah, S. H. Ahmad, S. F. Jusoh, A. A. Mansor, and S. A. A. Hamid, "Electromagnetic and absorption properties of some microwave absorbers," *Journal of Applied Physics*, vol. 92, pp. 876-882, 2002.

Vita

Jason Ray Cook, son of Billy Ray and Sun Ja Cook, was born Thursday, March 18, 1982 in Carlisle, PA. At the age of one he moved to Harlan, KY and remained until he graduated from Harlan High School in May, 2000. Jason attended the University of Kentucky in Lexington, KY for the next four years, majoring in mechanical engineering. Before graduating, he accepted a job as a research engineer with Delta M Corp., Oak Ridge, TN. His work was contracted to the Y-12 National Security Complex, Oak Ridge National Laboratories, Tennessee Eastman, and the Tennessee Valley Authority. While working with Delta M Corp., Jason attended the University of Tennessee, Knoxville, TN and completed a bachelor's degree in biomedical engineering in 2007. In the fall of 2007 he attended the University of Texas at Austin, Austin, TX to pursue a master's degree in biomedical engineering. From the summer of 2008 to the present, Jason is a Graduate Research Assistant in the Ultrasound Imaging and Therapeutics Research Laboratory.

Permanent Address: 7812 Shadowood Dr.
Knoxville, TN 37938

This thesis was typed by the author.